Available online at www.sciencedirect.com

ScienceDirect

Geochimica et Cosmochimica Acta 213 (2017) 137–154

Geochimica et Cosmochimica Acta

www.elsevier.com/locate/gca

Oxygen and U-Th isotopes and the timescales of hydrothermal exchange and melting in granitoid wall rocks at Mount Mazama, Crater Lake, Oregon

Meagan E. Ankney [a,*], Charles R. Bacon [b], John W. Valley [a], Brian L. Beard [a], Clark M. Johnson [a]

[a] Department of Geoscience, University of Wisconsin-Madison, 1215 West Dayton Street, Madison, WI 53706, United States
[b] U.S. Geological Survey Volcano Science Center, 345 Middlefield Road, Menlo Park, CA 94025, United States

Received 7 June 2016; accepted in revised form 10 April 2017; Available online 18 May 2017

Abstract

We report new whole rock U-Th and *in-situ* oxygen isotope compositions for partially melted (0–50 vol% melt), low-$\delta^{18}O$ Pleistocene granitoid blocks ejected during the ~7.7 ka caldera-forming eruption of Mt. Mazama (Crater Lake, Oregon). The blocks are interpreted to represent wall rocks of the climactic magma chamber that, prior to eruption, experienced variable amounts of exchange with meteoric hydrothermal fluids and subsequent partial melting. U-Th and oxygen isotope results allow us to examine the timescales of hydrothermal circulation and partial melting, and provide an "outside in" perspective on the buildup to the climactic eruption of Mt. Mazama. Oxygen isotope compositions measured in the cores and rims of individual quartz ($n = 126$) and plagioclase ($n = 91$) crystals, and for transects across ten quartz crystals, document zonation in quartz ($\Delta^{18}O_{Core\text{-}Rim} \leq 0.1$–$5.5‰$), but show homogeneity in plagioclase ($\Delta^{18}O_{Core\text{-}Rim} \leq \pm 0.8‰$). We propose that oxygen isotope zonation in quartz records hydrothermal exchange followed by high-temperature exchange in response to partial melting caused by injection of basaltic to andesitic recharge magma into the deeper portions of the chamber. Results of modeling of oxygen diffusion in quartz indicates that hydrothermal exchange in quartz occurred over a period of ~1000–63,000 years. Models also suggest that the onset of melting of the granitoids occurred a minimum of ~10–200 years prior to the Mazama climactic eruption, an inference which is broadly consistent with results for magnetite homogenization and for Zr diffusion in melt previously reported by others.

Uranium-thorium isotope compositions of most granitoid blocks are in ^{238}U excess, and are in agreement with a ^{238}U enriched array previously measured for volcanic rocks at Mt. Mazama. Uranium excess in the granitoids is likely due to enrichment via hydrothermal circulation, given their low $\delta^{18}O$ values. The sample with the highest U excess ($\geq 5.8\%$) also has the most ^{18}O isotope depletion (average $\delta^{18}O_{plag} = -4.0‰$). The granitoids are a probable assimilant and source of U excess in volcanic rocks from Mt. Mazama. Two granitoids have Th excess and low $\delta^{18}O$ values, interpreted to record leaching of U during hydrothermal alteration. A U-Th isochron based on the U excess array of the granitoids and volcanic rocks indicates that hydrothermal circulation initiated ~40–75 kyrs before the climactic eruption, potentially marking the initiation of a persistent upper-crustal magma chamber. The U-Th ages are consistent with the maximum timescales inferred for hydrothermal alteration based on oxygen isotope zoning in quartz.
© 2017 Elsevier Ltd. All rights reserved.

Keywords: Crater Lake; Mount Mazama; Cascade arc; Oxygen isotopes; Uranium-series isotopes; Caldera

* Corresponding author at: Department of Earth and Planetary Sciences, Northwestern University, Technological Institute, 2145 Sheridan Road, Evanston, IL 60208, United States.
E-mail address: meagan.ankney@northwestern.edu (M.E. Ankney).

http://dx.doi.org/10.1016/j.gca.2017.04.043
0016-7037/© 2017 Elsevier Ltd. All rights reserved.

1. INTRODUCTION

Assessment of the timescales of pre-eruptive processes in large, upper crustal, silicic magma chambers is essential to understanding the development of caldera systems and prediction of future eruptions. Upper crustal processes in magma chambers associated with caldera-forming eruptions are thought to occur over a variety of timescales (e.g., Saunders et al., 2010; Allan et al., 2013; Bindeman and Simakin, 2014). Studies suggest that large silicic magma bodies can persist in the upper crust as crystal mushes for $>10^5$ years (e.g., Brown and Fletcher, 1999; Vazquez and Reid, 2004; Simon and Reid, 2005; Bachmann et al., 2007; Folkes et al., 2011; Wotzlaw et al., 2013), and production of eruptible batches of magma has been interpreted to involve shorter timescales of 10^3-10^5 yrs (e.g., Allan et al., 2013; Bindeman and Simakin, 2014; Wotzlaw et al., 2013, 2014, 2015). Some recent studies, however, suggest that remobilization and final assembly of large scale silicic magma chambers might occur on more rapid timescales of decades to centuries prior to eruption (e.g., Wark et al., 2007; de Silva et al., 2008; Saunders et al., 2010; Druitt et al., 2012).

Ejecta of the caldera-forming eruption of Mt. Mazama (Crater Lake) include a minor component of granitoid blocks (as large as 4 m) that are interpreted to represent the wall rocks of the magma chamber, and hence offer a view of a shallow silicic magma chamber that is potentially distinct from that recorded in phenocrysts. Compositions and ages of the granitoids indicate they are plutonic remnants of Pleistocene dacite and rhyodacite magmas at Mt. Mazama (Bacon, 1992; Bacon et al., 2000; Bacon and Lowenstern, 2005). In this paper, we present an analysis of the temperature and hydrothermal history recorded in the granitoids using U-Th disequilibria and *in situ* oxygen isotope measurements. We propose that the most recent isotopic shifts in the granitoids reflect important thermal events in the growing magma chamber during the final buildup to the caldera-forming eruption. Our approach of using wall-rock samples to understand the development of the climactic magma chamber provides an "outside in" view that is complementary to that provided by phenocrysts in the magma chamber.

2. GEOLOGIC BACKGROUND AND PRIOR OXYGEN ISOTOPE STUDIES

Crater Lake caldera was formed by the climactic eruption of Mt. Mazama ca. 7.7 ka, and is one of only three Quaternary calderas in the Cascades (Bacon and Lanphere, 2006; Hildreth, 1996, 2007). Deposits of the climactic eruption are comprised of ~50 km^3 of primarily rhyodacitic magma that vented as pumice and ash. Other components of the climactic ejecta include andesitic scoria that has either relatively high incompatible (designated as high-Sr or "HSr" units) or comparatively low incompatible (designated as low-Sr or "LSr" units) element contents (terminology of Bacon and Druitt, 1988), mafic cumulates, and, of interest to this study, granitoid blocks that are interpreted to have been derived from the walls of the magma chamber. The granitoids are found in all deposits of the climactic eruption, but are concentrated in lithic breccia deposited within a few kilometers of the caldera during the later stages of the climactic eruption. Rare granitoid xenoliths are also found in preclimactic dacites and rhyodacites erupted from ~7.8 ka to 70 ka (Bacon et al., 1994), but these were not analyzed in this study. Collectively, they consist mainly of granodiorite, with minor quartz diorite, aplite, granite, diabase, and granophyre. Hereafter we will use the terms "granitoids" or "granitoid blocks" to refer to all varieties of felsic plutonic blocks at Crater Lake.

The granitoid blocks are interpreted to have experienced variable amounts of subsolidus exchange with meteoric hydrothermal fluids and, in many cases, were partially melted (Bacon et al., 1989, 1994; Bacon, 1992). Zircon geochronology indicates that the granitoids reflect crystallization of plutonic bodies between ~300 ka and 20 ka (Bacon and Lowenstern, 2005). Ages of zircons cluster around three time periods at 50–70 ka, ~110 ka, and ~200 ka, each of which corresponds to a period of dacitic volcanism at Mt. Mazama (Bacon and Lowenstern, 2005). The granitoids and related rocks are considered to represent the non-erupted portions of the magma chamber(s) that produced the dacites.

Granitoid blocks from the climactic eruption show partial melting up to 50 vol.%, as indicated by the presence of intergranular high-silica rhyolite glass that represents quenched melt (Bacon, 1992). The absence of granitoids that experienced >50% partial melting, which is above the threshold for the onset of plastic flow (Arzi, 1978; Marsh, 1981; Bacon et al., 1989), likely reflects disaggregation and assimilation by the climactic magma (Bacon et al., 1989; Bacon, 1992). Fe-Ti oxides in partially melted samples that are in contact with intergranular glass are thought to have re-equilibrated with the melt and give Fe-Ti oxide equilibration temperatures of 760–1010 °C (Bacon, 1992). Many of the oxide temperatures exceed those obtained for oxide phenocrysts in the rhyodacite and later-erupted andesitic scoria and mafic cumulates (examples of the latter that lack ilmenite may have been hotter still), suggesting that granitoid blocks may have been from the walls of the deeper portions of the chamber, consistent with the higher concentration of blocks in later products of the caldera-forming eruption (Druitt and Bacon, 1989; Bacon, 1992). Fe-Ti oxides in nonmelted samples, and those not in contact with glass in partially melted samples or are present as mineral inclusions, give temperatures of 690 °C to 830 °C, and probably document initial crystallization conditions (Bacon, 1992).

Previous work on bulk mineral separates of plagioclase, quartz, and glass from granitoid blocks found in deposits of the climactic eruption and in preclimactic rhyodacite/dacite lavas demonstrates a wide range in oxygen isotope compositions, with $\delta^{18}O$ values ($\delta^{18}O = [(({}^{18}O/{}^{16}O)_{sample}/({}^{18}O/{}^{16}O)_{standard} - 1) \times 1000]$ where the standard is VSMOW) that range from $\delta^{18}O_{plag} = +6.5‰$ to $-3.4‰$, $\delta^{18}O_{quartz} = +8.0‰$ to $-2.2‰$, and $\delta^{18}O_{glass} = +4.1‰$ to $+2.9‰$ (Bacon et al., 1989, 1994). The majority of the granitoid blocks have $\delta^{18}O$ values that are considerably lower

than those expected for mantle-derived magmas. Bacon et al. (1989) interpreted the low-$\delta^{18}O$ values to reflect exchange with Pleistocene meteoric hydrothermal fluids followed by high-temperature exchange during heating and/or partial melting. Hydrothermal circulation is thought to have initiated between 70 and 27 ka, based on the presence of a granitoid clast that has "normal" $\delta^{18}O$ values in the dacite of Pumice Castle erupted at 70 ka (Bacon et al., 1994). The presence of low-$\delta^{18}O$ glass in the partially melted blocks indicates that oxygen isotope exchange between meteoric waters and the plutonic bodies occurred prior to melting. The relatively wide range in $\delta^{18}O$ values, ~10‰, measured in the granitoids presumably records a range of water/rock mass ratios (Bacon et al., 1989).

Oxygen isotope fractionation between bulk quartz, plagioclase, and glass separates is consistent with high-temperature re-equilibration of the granitoids during heating and/or partial melting (Bacon et al., 1989). Quartz-plagioclase fractionation tends to decrease with increasing Fe-Ti oxide temperatures (760–1000 °C for oxides that re-equilibrated during partial melting), which in turn correlates with increasing percent melting (Bacon et al., 1989; Bacon, 1992). The range in Fe-Ti oxide temperatures is thought to relate to storage depth; the granitoids that equilibrated to higher temperatures were likely located in the deepest, hottest portions of the walls of the magma chamber. Alternatively, the range in temperatures may reflect proximity of the blocks to the magma chamber, in which case lower temperatures may be indicative of storage farther back in the walls of the chamber.

The presence of granitoid blocks in deposits of the caldera-forming eruption and their bulk mineral/glass oxygen isotope compositions provide evidence for upper crustal assimilation by the magma chamber at Crater Lake. Rhyodacites erupted from the climactic magma chamber have bulk $\delta^{18}O$ values for plagioclase of +6.0 to +6.5‰. These are ~0.5–1‰ lower than expected values, which, when taken into consideration with other trace-element, isotopic, and petrographic data, are suggestive of up to ~25% assimilation of low-$\delta^{18}O$, upper crustal material for an assimilant with a $\delta^{18}O_{plag}$ value of +5.0‰ (Bacon et al., 1989, 1994).

3. PETROLOGY OF THE SAMPLE SUITE

Samples of granitoid blocks selected for this study were collected during geologic mapping of the Mt. Mazama region (Bacon, 2008). All of the samples have been analyzed for major- and trace-element geochemistry. Five were analyzed with X-ray fluorescence (XRF) and instrumental neutron activation analysis (INAA) by Bruggman et al. (1987), and the remaining two were analyzed via inductively coupled plasma optical emission spectrometry (ICP-OES) and inductively coupled plasma mass spectrometry (ICP-MS) by Activation Laboratories Ltd. (ActLabs) for this study. Six of the seven samples analyzed are granodiorite and the remaining sample is aplite. The samples represent the full range of partial melting observed in the granitoids from 0 to 50 vol.%. Plagioclase (≤6 mm diameter in nonmelted samples) display oscillatory zoning and range in composition from An_{13} to An_{67} (Bacon, 1992). Cores tend to be ≤ An_{50} and are typically more calcic than rims. Quartz (≤1.5 mm in nonmelted samples) grew in the interstitial space surrounding the plagioclase and is accompanied by alkali feldspar and sodic plagioclase crystals, commonly in granophyric intergrowths (Bacon, 1992). Cathodoluminescence (CL) images of the quartz crystals reveal magmatic growth zoning, as well as evidence for alteration and heating in the form of overgrowths, healed cracks, and dark, possibly recrystallized zones. Other minerals include hypersthene, augite, hornblende, biotite, magnetite, ilmenite, apatite, and zircon (Bacon, 1992). Zircons analyzed in this study have SHRIMP ^{238}U-^{230}Th model ages of ~ 110–200 ka (sample 1627) and ~ 27 ka (sample 1995), and span nearly the full range of crystallization ages represented by the granitoids and associated antecrystic zircons (Bacon and Lowenstern, 2005).

4. ANALYTICAL METHODS

4.1. *In situ* oxygen isotope analysis

To prepare the granitoids for *in situ* oxygen isotope analysis, rock chips of six samples were cut using a thin diamond saw blade and were cast in 2.5 cm diameter epoxy plugs. Two grains of UWQ-1, a well-characterized quartz reference standard for SIMS oxygen isotope analysis (Kelly et al., 2007), were embedded with epoxy in shallow,<2 mm holes drilled near the center of each sample round. The 2.5 cm rounds were polished using a procedure outlined by Heck et al. (2011) to minimize sample surface relief, which is key to obtaining accurate and precise isotope ratio analyses via SIMS (Kita et al., 2009, 2011). Zircon grain mounts that were previously used for *in situ* U-Th isotope analyses (Bacon et al., 2000; Bacon and Lowenstern, 2005) were used for oxygen isotope analysis by SIMS in this study. These mounts include zircons from nonmelted sample 1627 and minimally melted sample 1995 (<2% melt). We note that targeting zircons only from nonmelted to minimally melted samples avoids the potential for dissolution of zircon rims during partial melting of the granitoids. To prepare the zircon mounts for SIMS analysis, 4 to 5 grains of KIM-5, a well-characterized zircon reference standard (Valley, 2003), were embedded near the center of the mounts. The samples were then re-polished following the procedure above.

Samples were imaged in preparation for SIMS analysis with a Hitachi S-3400 N scanning electron microscope (SEM) using secondary electron (SE), back-scattered electron (BSE), and cathodoluminescence (CL) imaging. Spot analyses to confirm the identity of mineral phases were performed using Energy-Dispersive X-ray Spectroscopy (EDS) at an accelerating voltage of 15 keV, a working distance of 10 mm, and Thermo Scientific NORAN System SIX software. The samples were also imaged by SEM after SIMS analysis to evaluate the ion probe pits for the presence of inclusions, cracks, or other irregularities.

In situ oxygen isotope analyses of cores and rims of plagioclase, quartz, and zircon (Table A1 in Appendix A) were performed on the CAMECA IMS-1280 secondary ion mass

spectrometer (SIMS) at the WiscSIMS Laboratory at the University of Wisconsin-Madison Department of Geoscience. In addition, detailed core to rim transects were measured across a total of ten quartz crystals in a nonmelted granitoid and four of the partially melted granitoids. Analysis spots were selected based on detailed SE, BSE, and CL images with the goal of avoiding cracks, inclusions, and other defects in the crystal surface. Because increased uncertainty can be introduced by instrumental mass bias ("XY effect", Kita et al., 2009), the spots, which are approximately 10 to 20 μm in diameter, were placed within 8 mm of the center of the sample round (Peres et al., 2013). Instrumental mass fractionation (IMF or bias) and drift were monitored and corrected by performing 4–5 analyses of the UWQ-1 quartz standard in the granitoid sample rounds and the KIM-5 zircon standard in the zircon grain mounts before and after every 10–15 analyses of unknowns. A detailed description of this bracketing method can be found in Valley and Kita (2009). Precision (2SD) for the unknown analyses were calculated based on the standard deviation of the bracketing standard analyses collected before and after each group of unknowns. To determine instrumental bias correction factors for plagioclase, measurements of $\delta^{18}O$ were collected in homogenous plagioclase standards of known oxygen isotope compositions and then used to generate a calibration curve relative to the UWQ-1 quartz standard (Valley and Kita, 2009). Because instrumental bias varies with anorthite (An) content, correction factors were determined for plagioclase standards with a range of An content, from An_0 to An_{90} (see Appendix C). To apply this correction to plagioclase in the samples, An content was measured for the SIMS analysis spots using a CAMECA SX51 and Probe for Windows software in the Eugene Cameron Electron Microprobe Lab at the University of Wisconsin-Madison Department of Geoscience. All $\delta^{18}O$ values are reported relative to VSMOW.

4.2. U-Th isotopes

Samples selected for U-Th isotope analysis include the six granodiorites analyzed for oxygen isotopes as described above and an additional granitic aplite sample. Aliquots of ~ 125–200 mg of powdered whole rock were dissolved and processed to separate U and Th using methods described in Wende et al. (2015). Uranium-series isotope ratios were measured on a Micromass *Isoprobe* MC-ICP-MS at the University of Wisconsin-Madison's ICP-TIMS Lab, Department of Geoscience, following methods of Ankney et al. (2013) and Jicha et al. (2009). Uranium and Th cuts of each sample were prepared for isotopic analysis and analyzed as described in Ankney et al. (2013). External precision, reproducibility, and accuracy of Th and U isotope measurements were monitored through analyses of spiked and nonspiked rock standards (AGV-2, BCR-2) and U and Th standard solutions (IRMM-035, IRMM-036, NBL-114, U-500). For Th isotope analysis, a second-order polynomial correction ($R^2 > 95\%$) based on the $\delta^{232}Th/^{230}Th$ values (the measured $^{232}Th/^{230}Th$ relative to IRMM) and total ion intensity was applied to the data. Thirty-seven analyses of IRMM-035 yielded a $^{232}Th/^{230}Th$ ratio of 87,817 ± 0.39%, 42 analyses of IRMM-036 yielded a $^{232}Th/^{230}Th$ ratio of 326,784 ± 0.80%, 11 analyses of BCR-2 yielded a $^{232}Th/^{230}Th$ ratio of 211,331 ± 0.72%, and 13 analyses of AGV-2 yielded a $^{232}Th/^{230}Th$ ratio of 196,292 ± 0.69%. These measured values are indistinguishable from consensus values given by Sims et al. (2008). U-Th concentrations and isotopic compositions for the rock standards are given in Table 1.

5. RESULTS

5.1. Oxygen isotope results

In situ oxygen isotope analysis of core to rim variations in plagioclase and quartz reveal distinct variations between these minerals (Table A1 in Appendix A). Cores and rims of plagioclase ($n = 91$) are typically homogeneous within analytical uncertainty (≤0.3‰; Fig. 1A). Oxygen isotope analyses in quartz cores and rims ($n = 126$), however, show that quartz in both nonmelted and partially melted granitoids is typically zoned, where the difference in $\delta^{18}O$ values between core and rim ($\Delta^{18}O_{core\text{-}rim}$) can be up to 5.5‰, although most are significantly smaller (≤~0.5‰) (Fig. 1B). Core-to-rim transects measured across ten quartz grains ($\Delta^{18}O_{core\text{-}rim}$ from 0.3 ± 0.3‰ to 5.5 ± 0.3‰) reveal oxygen isotope zoning profiles in which $\delta^{18}O$ values drop from the cores towards the rims (see Fig. 2 and Figs. B1–B9 in Appendix B). Transects measured at multiple orientations across crystals in nonmelted sample 1627 reveal fairly symmetrical zoning patterns with respect to the $\delta^{18}O$ values measured for the rims and the slope of oxygen isotope profiles within individual crystals (Figs. B1–B3 in Appendix B). In partially melted samples, $\delta^{18}O$ values measured at multiple points around the rim of individual crystals are also typically the same and do not vary beyond the analytical uncertainty of the SIMS measurements (Fig. 2 and Figs. B4–B9 in Appendix B). Importantly, embayment of the rims by melting typically does not appear to truncate the measured profiles, and steeper oxygen isotope profiles are measured parallel to the direction of melting (Fig. 2).

In situ oxygen isotope analyses of cores and rims of zircons ($n = 26$) for two of the samples analyzed in this study (nonmelted sample 1627 and minimally melted sample 1995) give $\delta^{18}O$ values from 5.2 ± 0.2‰ (rim) to 6.0 ± 0.3‰ (rim) (Table A1 in Appendix A, Fig. B11 in Appendix B), which are consistent with "normal" magmatic $\delta^{18}O$ for zircon, i.e., similar to values in high temperature equilibrium with the mantle (Valley, 2003).

5.2. U-Th isotope results

The majority of whole-rock granitoid samples analyzed in this study display U-Th disequilibrium with ^{238}U excess (Fig. 3) and define a trend that coincides with U-Th isotope compositions measured in pre-climactic and climactic rhyodacites and dacites and LSr scoria erupted during the climactic eruption (Fig. 4, Ankney et al., 2013). Activity ratios of ($^{230}Th/^{232}Th$) were corrected for the ingrowth of

Table 1
U-Th isotope data for granitoid blocks from Mt. Mazama.

Sample	Material	SiO_2 wt.%	$(^{238}U/^{232}Th)$	2SE	$(^{230}Th/^{232}Th)$	2SE	$(^{230}Th/^{232}Th)_0$[a]	Th (ppm)	U (ppm)	*n*	Bulk $\delta^{18}O$ (‰ VSMOW)[b]
Granitoids											
1627	wr	67.6	1.297	0.008	1.365	0.008	1.370	4.84	2.07	1	5.1q, 2.8p
1995	wr	68.2	1.447	0.009	1.402	0.008	1.399	3.96	1.89	1	–
452	wr	63.3	1.536	0.009	1.458	0.009	1.452	3.45	1.75	1	−2.2q, −3.7p
1326	wr	68.1	1.407	0.008	1.382	0.008	1.380	4.39	2.03	1	3.8q, 2.8p, 2.9 g
1038	wr	67.4	1.391	0.008	1.380	0.008	1.379	4.22	1.94	1	3.0q, 2.1p, 2.6 g
1023	wr	67.3	1.406	0.008	1.387	0.008	1.385	4.24	1.97	1	4.9q, 4.2p, 4.1 g
432	wr	73.1	1.353	0.008	1.392	0.008	1.395	9.92	4.42	1	0.6q, 0.8p
Whole-rock standards											
AGV-2	wr std	–	0.938	0.003	0.943	0.007	–	6.04	1.87	13	–
BCR-2	wr std	–	0.869	0.002	0.876	0.006	–	5.87	1.68	12	–

[a] Initial Th isotope ratios calculated using an age of 7.7 ka.
[b] Most bulk data for plagioclase (p), quartz (q), and glass (g) from Bacon et al. (1989). Bulk plagioclase values for samples 1627 and 452 measured at UW-Madison.

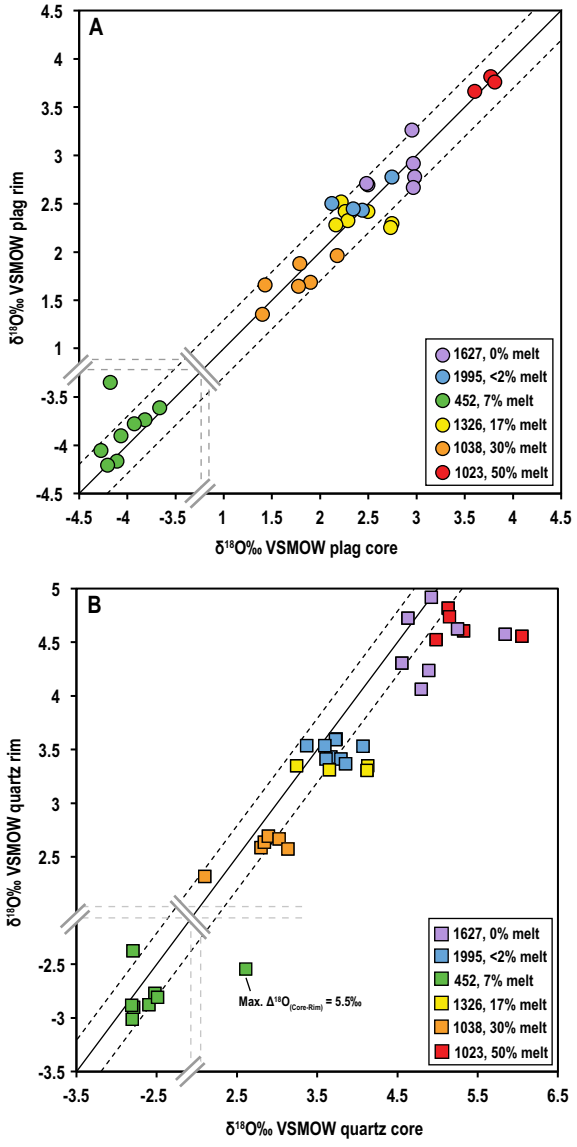

Fig. 1. $\delta^{18}O$ (‰ VSMOW) values for minerals in partially melted granodiorites from the climactic deposits of Mt. Mazama, Crater Lake, Oregon. The solid line indicates a 1:1 relation and the dotted lines denote the average 2SD of the *in situ* oxygen isotope analyses (0.3‰). Averages are shown for crystals in which multiple core and/or rim points were measured. A complete set of core and rim points is plotted in Fig. B12 of Appendix B. (A) $\delta^{18}O$ values for plagioclase cores relative to rims. Plagioclase crystals typically have no significant core to rim zonation in their oxygen isotope compositions, and, where zonation does exist, there is no discernable pattern with respect to a systematic direction of change in $\delta^{18}O$ toward the rim. (B) $\delta^{18}O$ values for quartz cores relative to rims. Quartz cores tend to be heavier relative to rims (typically $\Delta^{18}O_{core\text{-}rim} \leq 0.5‰$), with a maximum $\Delta^{18}O_{core\text{-}rim}$ fractionation of 5.5‰ in sample 452 (7% melt).

^{230}Th since the time of eruption using an age of 7.7 ka, as this represents the minimum possible age of the granitoids and any glass (quenched melt) present in them. Ages of 20–200 ka are proposed as possible crystallization ages for the granitoids based on U-Th zircon geochronology

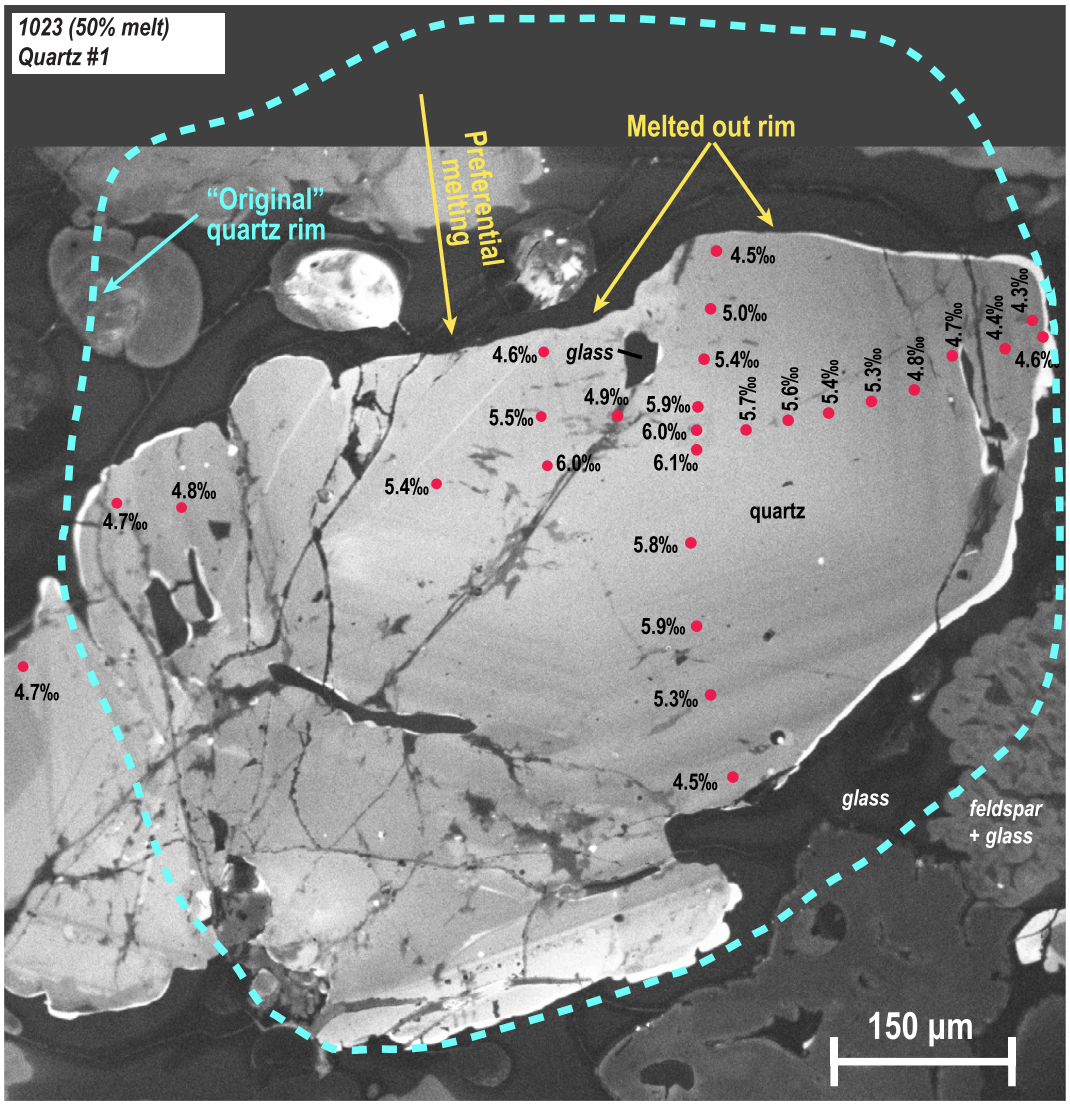

Fig. 2. Transects measured via SIMS shown across a cathodoluminescence (CL) image of quartz crystal (Q1) in partially melted granitoid 1023. An estimated outline of the original crystal margins is shown, as well as preferential shortening of measured profiles along the top edge by melting. The horizontal transect across the right half of the grain is plotted in Fig. 8D. Images of transects measured across additional crystals are shown in Figs. B1–B9 of Appendix B.

(Bacon and Lowenstern, 2005). The maximum U excess recorded in the granitoids ranges from 5.8% to 8.8%, based on ages of 7.7 ka and 50 ka, respectively. Because the granitoids have exchanged with hydrothermal fluids, it is possible that additional ingrowth of ^{230}Th may have occurred from decay of excess ^{234}U (i.e., (^{234}U/^{238}U) > 1) added via hydrothermal fluids, which could skew the apparent ages of the granitoids by up to 30 kyr (see Ankney et al., 2013). It is important to note, however, that these calculations represent a maximum effect of ^{234}U excess in hydrothermally altered rocks, and that Villemant et al. (1996) indicate that (^{234}U/^{238}U) ratios can be unaffected by interaction with hydrothermal systems, even in samples that have strong enrichments in ^{238}U relative to ^{230}Th due to interaction with hydrothermal fluids (e.g., Sturchio et al., 1987). We therefore suggest that ^{234}U excess did not have a significant effect on the (^{230}Th/^{232}Th) ratio of the granitoids, especially because they have relatively small U excesses.

Two of the samples (1627 and 432) analyzed in this study plot in ^{230}Th-excess in Fig. 3. Sample 1627 is a non-melted granodiorite that has ≥5.6% Th-excess, based on a minimum (^{230}Th/^{232}Th) correction age of 7.7 ka. Cathodoluminescence images of quartz in this sample reveal a large network of annealed fractures and CL-dark zones (Fig. B10 in Appendix B). Sample 432 is a partially melted granitic aplite that has ≥3.0% Th-excess. Its major- and trace-element compositions indicate that it is significantly more differentiated than the granodiorites, and it has no eruptive equivalent at Mt. Mazama (Bacon, 1992).

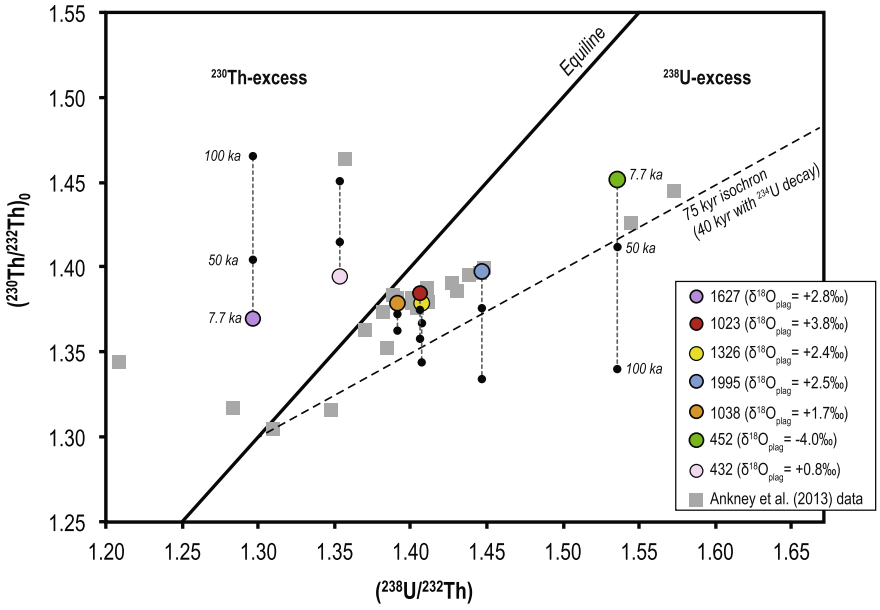

Fig. 3. U-Th isotope data for the granitoids analyzed in this study and previously published data for Mt. Mazama. $(^{230}Th/^{232}Th)_0$ ratios for the colored circles were age-corrected using a baseline age of 7.7 ka (the climactic eruption), which is the minimum possible age for the granitoids. The black circles represent the Th isotope compositions if an age of 50 or 100 ka is assumed. Comparing the results from the granitoids to earlier work on eruptive units by Ankney et al. (2013) suggests that U-Th ages of ~7.7–50 ka provide the best fit for the existing Crater Lake data for the volcanic component, and this U-Th age range is inferred for the granitoids measured in this study. The black line represents the 40–75 kyr isochron of Ankney et al. (2013). Colors of symbols match those in Fig. 1. (For interpretation of the references to color in this figure legend, the reader is referred to the web version of this article.)

6. DISCUSSION

Given the low $\delta^{18}O$ values of meteoric water in the region (present day: ~−14‰ VSMOW, Thompson et al., 1987), oxygen isotopes are particularly sensitive tracers of upper crustal processes associated with growth of the climactic chamber at Mt. Mazama (Bacon et al., 1989, 1994). Based on prior U-Th isotope studies at Crater Lake (Ankney et al., 2013), U-series isotopes provide constraints on the timing of upper crustal hydrothermal interaction. In the discussion below, we first use models of oxygen diffusion under hydrothermal conditions and the U-Th isotope composition of the granitoids to assess the timing of hydrothermal circulation associated with the climactic magma chamber. Oxygen isotope diffusion models are then used to examine timescales of partial melting in the granitoids in an attempt to understand the origin of the most highly melted granitoids in the context of the climactic magma chamber as envisaged by Druitt and Bacon (1989).

6.1. Evidence for two stages of oxygen isotope exchange in wall rocks at Mt. Mazama

In situ measurements of oxygen isotope compositions in plagioclase, quartz, and zircon crystals in this study provide a record of a minimum of two stages of oxygen isotope exchange that affected the granitoid wall rocks surrounding the climactic magma chamber at Mt. Mazama (Fig. 4). We propose that these stages can be distinguished based on differences observed in the oxygen isotope zonation and fractionation measured in nonmelted or incipiently melted samples relative to those containing significant proportions of melt. An initial, subsolidus exchange stage can be inferred from the presence of zircon crystals with mantle-like $\delta^{18}O$ values in nonmelted sample (1627) and minimally melted sample 1995 (<2% melt), which indicates that the parent magmas did not originally have unusually low $\delta^{18}O$ values (see Fig. B11 in Appendix B). Lowering of $\delta^{18}O$ values in plagioclase and quartz in these samples therefore requires oxygen isotope exchange after the granitoids initially crystallized, as was suggested by Bacon et al. (1989). Hereafter, we refer to this subsolidus exchange as Exchange Stage 1 and interpret the resulting low $\delta^{18}O$ values in plagioclase and quartz to reflect hydrothermal circulation of low-$\delta^{18}O$ meteoric waters, which seems likely to have occurred through fluid flow along grain boundaries and fast grain boundary diffusion (e.g., Eiler et al., 1992). Exchange Stage 1 is best represented by the $\delta^{18}O$ zonation observed across core to rim transects in quartz in sample 1627 (Fig. 4). This sample is nonmelted and is therefore least likely to have been affected by significant (i.e., measureable via SIMS) high temperature exchange during later heating that resulted in partial melting of most granitoid samples. Moreover, the $\Delta^{18}O_{qtz\text{-}plag}$ fractionation (using quartz rims) of ~1.6‰ measured for this sample is consistent with exchange at subsolidus temperatures of ~450–650 °C (e.g., Matthews et al., 1983; Chiba et al., 1989) and thus under hydrothermal conditions.

Two lines of evidence suggest that a second stage of oxygen isotope exchange took place during heating and melting of the granitoid blocks, defined here as Exchange Stage 2. First, $\Delta^{18}O_{qtz\text{-}plag}$ and $\Delta^{18}O_{qtz\text{-}glass}$ fractionations are

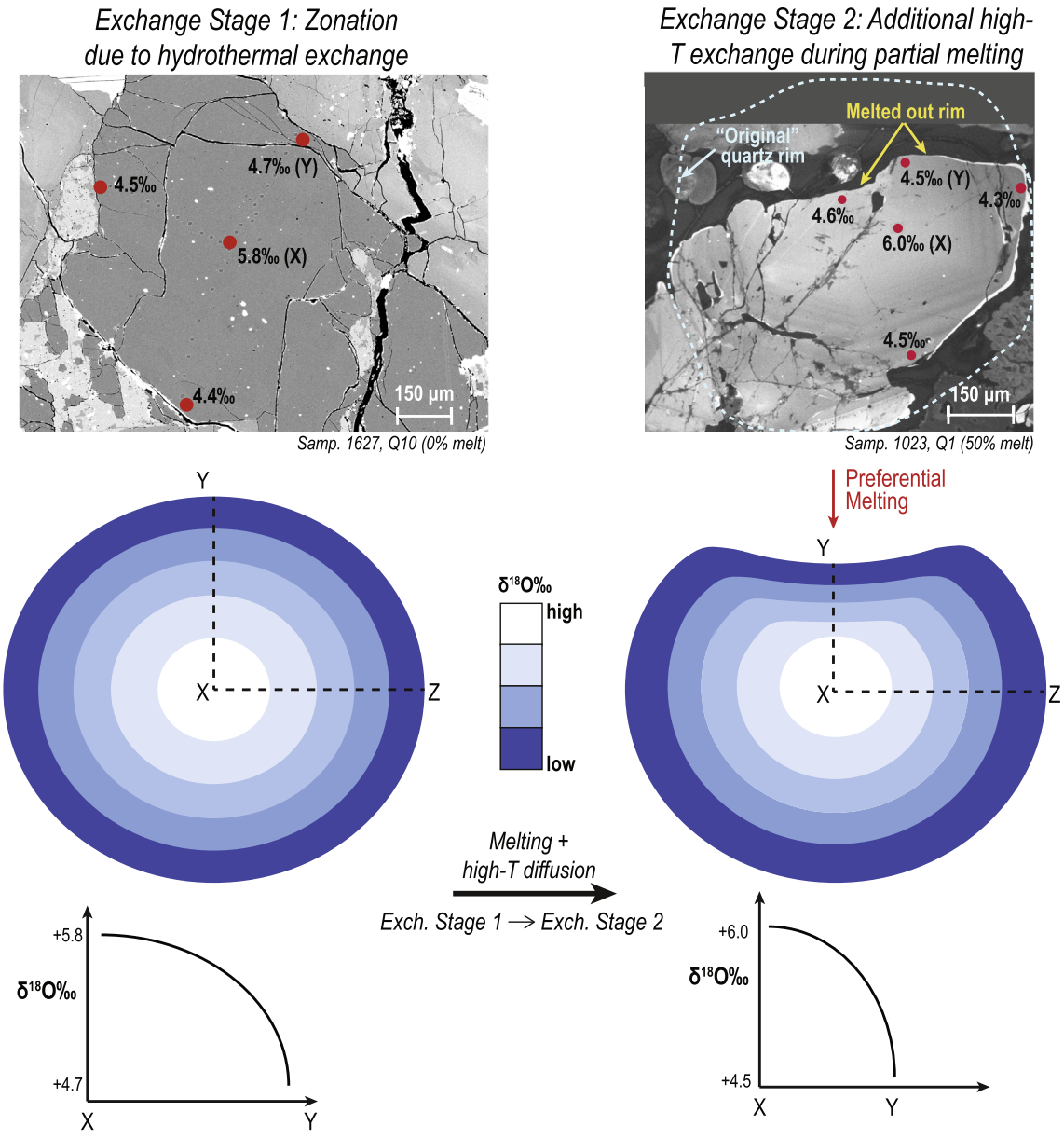

Fig. 4. Schematic diagram showing the results of diffusion during both Exchange Stage 1 (hydrothermal) and Exchange Stage 2 (partial melting). The crystal shown for Exchange Stage 1 is from nonmelted sample 1627 and the crystal for Exchange Stage 2 is from partially melted sample 1023. For simplicity, only the core and rim values are shown on the image of each crystal. Complete measured transects are available in Fig. B3 of Appendix B for sample 1627 and Fig. 2 for sample 1023.

significantly smaller at ~0.0–1.2‰ (using quartz rims) in the melted samples relative to those in the nonmelted sample (1627), indicating additional oxygen isotope exchange took place at high temperatures (e.g., Bindeman and Valley, 2002). Second, petrographic evidence exists in the partially melted granitoids for the influence of melting on oxygen isotope profiles. Melting at the edges of the crystals generally does not truncate the measured diffusion profiles. Where melting preferentially affected one side of a crystal, we observe shortening and steepening of the diffusion profiles (Figs. 2 and 4). In the few cases where melting does appear to truncate the oxygen isotope gradients measured in quartz, this may be a result of melting and diffusion processes occurring concurrently and at different rates. Importantly, the preservation of diffusion profiles indicates that partial melting of the granitoid blocks was relatively rapid and thus occurred closely in time to the climactic eruption. This is quantified in Section 6.3.

The homogeneity in $\delta^{18}O$ values in the plagioclase cores and rims in both the nonmelted and partially melted granitoid blocks indicates that complete oxygen isotope diffusional relaxation occurred in plagioclase prior to the climactic eruption. Given the fact that oxygen diffusion coefficients for plagioclase at the temperatures of the climactic magma chamber are 5–30 times larger (i.e., faster) than those of quartz (Giletti et al., 1978;

Elphick et al., 1988), re-equilibration for plagioclase the size of crystals in the granitoids is expected except for short time scales ($\ll 10^2$ years).

6.2. Timescales for hydrothermal exchange (Exchange Stage 1)

6.2.1. Parameters for modeling hydrothermal exchange (Exchange Stage 1)

The presence of oxygen isotope zonation in quartz allows us to place constraints on the timescales of both hydrothermal exchange (Exchange Stage 1) and partial melting (Exchange Stage 2) of the granitoid blocks. To determine the amount of time (t_{hydro}) required to generate the measured profiles created during Exchange Stage 1 in the nonmelted sample (sample 1627), we reproduced the oxygen isotope zonation across each transect using a spherical model given by equation 6.18 from Crank (1975):

$$\frac{C - C_1}{C_0 - C_1} = 1 + \frac{2a}{\pi r}\sum_{n=1}^{\infty}\frac{(-1)^n}{n}\sin\frac{n\pi r}{a}e^{\left(-\frac{Dn^2\pi^2 t}{a^2}\right)} \quad (1)$$

where C is the composition at distance r (measured from center) in a sphere, C_1 is the initial composition, C_0 is the composition at the sphere's surface, a is the radius, D is a diffusion coefficient (discussed below), and t is time. This equation is for a simplified case of diffusion in a sphere where the isotopic composition of the diffusing element (e.g., $^{18}O/^{16}O$) remains constant at the surface of the sphere (Crank, 1975). We note that this assumes that the nonmelted sample did not undergo any high-temperature exchange in association with heating by the climactic magma chamber during Exchange Stage 2 before being erupted. It is unlikely that this assumption is completely correct, but, as noted previously, the amount of diffusive exchange during Exchange Stage 2 might have been small and not detected along measured traverses in sample 1627. Eq. (1) was also used to generate estimated Exchange Stage 1 profiles for the partially melted samples, which are in turn used as initial conditions for Exchange Stage 2.

Our diffusion models are primarily controlled by experimentally determined values of diffusion coefficients (D) for oxygen self-diffusion (volume diffusion), which is likely the rate-limiting step in isotopic exchange for these samples (e.g., Bacon et al., 1994; Valley, 2001). To calculate timescales for diffusion in quartz during Exchange Stage 1, we used diffusion coefficients determined for hydrothermal conditions ($P_{H2O} = 100$ MPa) by Dennis (1984), commensurate with the hydrothermal environment required to lower the $\delta^{18}O$ values of the samples from the presumed magmatic values indicated by zircon oxygen isotope compositions and typical zircon-melt oxygen isotopic fractionation (e.g., Bindeman and Valley, 2002). Diffusion coefficients for exchange during Exchange Stage 1 were then adjusted for different temperatures using the Arrhenius relation:

$$D = D_0 e^{-E/RT} \quad (2)$$

where D_0 is the pre-exponential factor (cm^2/s or m^2/s, determined experimentally), E is the activation energy (J/mol, determined experimentally), R is the gas constant (8.3143 J/K mol), and T is temperature (K). A range of temperatures of 400–700 °C was considered for Exchange Stage 1, which produces considerable variability in the t_{hydro} needed to model the measured profiles. Reproducing the $\delta^{18}O$ value measured for the core of a crystal in nonmelted sample 1627 requires a $t_{hydro} = \sim 10^3$ yrs at 700 °C and $t_{hydro} > 2 \times 10^6$ yrs at 400 °C (Fig. 5). At temperatures of $<\sim$510 °C, modeled times are too long based on the maximum age of the granitoids determined by zircon geochronology ($\sim$300 ka, Bacon and Lowenstern, 2005) or the maximum age for the onset of Exchange Stage 1 of $\sim$70 ka based on the presence of a "normal" $\delta^{18}O$ granitoid in eruptive products of that age (Bacon et al., 1994); we therefore restrict our discussion below to modeling using temperatures of >510 °C.

The amount of time required to produce the oxygen isotope gradients measured in quartz in this study is also dependent on the crystal size (diffusion distance, a) and the initial (C_1) and surface (C_0) $\delta^{18}O$ values (Valley, 2001). For our models, we set the diffusion distance (a) equal to the core-to-rim distance for each transect that we measured, which ranged from $\sim$100 to 450 μm. This may, however, underestimate t_{hydro} for Exchange Stage 1 in the partially melted samples, as the crystals are expected to be smaller than they were prior to melting. To evaluate possible effects of partial melting, the relation between t_{hydro} and crystal size at 510 °C is plotted in Fig. 6, which typically increases with increasing crystal diameter. Exceptions to this are two crystals found in partially melted samples 1023 and 1995 (Q6 in 1023 and Q7 in 1995, Fig. 6) that require relatively long timescales for Exchange Stage 1 despite their smaller size. These crystals have anomalously low $\delta^{18}O$ values in their cores (i.e., they require longer t_{hydro} to produce) that were likely lowered by diffusion during Exchange Stage 2, as discussed below. It is also important to note that the range of t_{hydro} calculated for single samples could be a result of the three-dimensional orientation or shape of the quartz crystals in the sample mount. Our

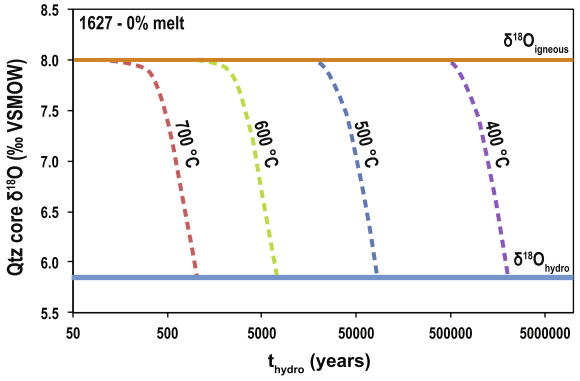

Fig. 5. Variability in t_{hydro} needed to reproduce the $\delta^{18}O$ value in the core of nonmelted sample 1627 at temperatures of 400–700 °C, where $\delta^{18}O_{igneous}$ represents the oxygen isotope composition in the core prior to Exchange Stage 1 and $\delta^{18}O_{hydro}$ represents the oxygen isotope composition following Exchange Stage 1.

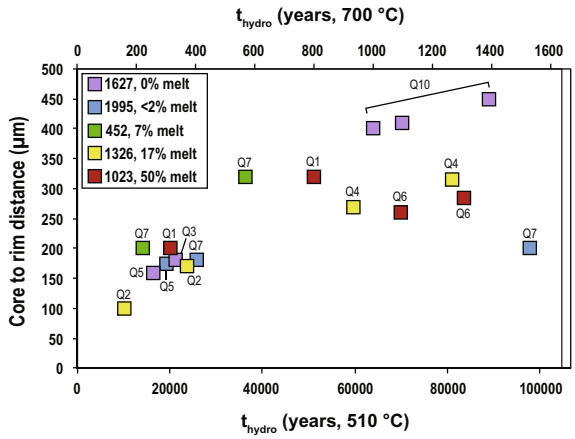

Fig. 6. Variability in t_{hydro} relative to crystal diameter for temperatures of 510 °C and 700 °C. Maps of transects measured across individual crystals are available in Appendix B.

models are limited by measuring transects for a single, two-dimensional cross section of each quartz crystal and thus actual distances to the rim of each grain could have been less than the distance given in Fig. 6.

The initial value (C_1) for quartz was assumed to be +8.0‰, which is in high-temperature equilibrium with zircon in these samples at magmatic temperatures. For the nonmelted sample, a re-equilibrated (rim) $\delta^{18}O$ value (C_0) was estimated by extrapolating the measured profiles to a distance of zero from the rim along the core-to-rim transverse. The re-equilibrated $\delta^{18}O$ values (C_0) for quartz for Exchange Stage 1 in the partially melted samples were calculated by adding 1.4‰, a value based on the $\Delta^{18}O_{qtz\text{-}plag}$ fractionation used for our model for the nonmelted sample, to the average $\delta^{18}O$ value measured for plagioclase in each sample. This assumes that the plagioclase crystals were homogenized to their current oxygen isotope composition during hydrothermal exchange in Exchange Stage 1, and were not significantly affected by subsequent high-temperature exchange during Exchange Stage 2. This assumption is probably an oversimplification, as it is likely that the $\delta^{18}O$ values for plagioclase were somewhat lower and/or the plagioclase crystals were zoned like the quartz prior to melting. Importantly, the C_0 values and modeled oxygen isotope profiles for Exchange Stage 1 for the partially melted samples must be distinct from the nonmelted sample because the $\delta^{18}O$ values for quartz and plagioclase in nonmelted sample 1627 are too low to be used to represent Exchange Stage 1 in partially melted sample 1023 (Fig. 7a). For our models, Exchange Stage 1 diffusion in the partially melted samples was presumed to have progressed until the $\delta^{18}O$ value in the core of each crystal matched either the maximum value measured for the core or the estimated C_0 for that sample (Fig. 7b). This approach gives a maximum t_{hydro} for each transect, as it assumes that the cores were not affected by subsequent diffusion during Exchange Stage 2, and, in conjunction with the variable C_0 values, produces modeled Exchange Stage 1 oxygen isotope profiles that vary between samples (blue curves in Fig. 8). A summary of temperature and

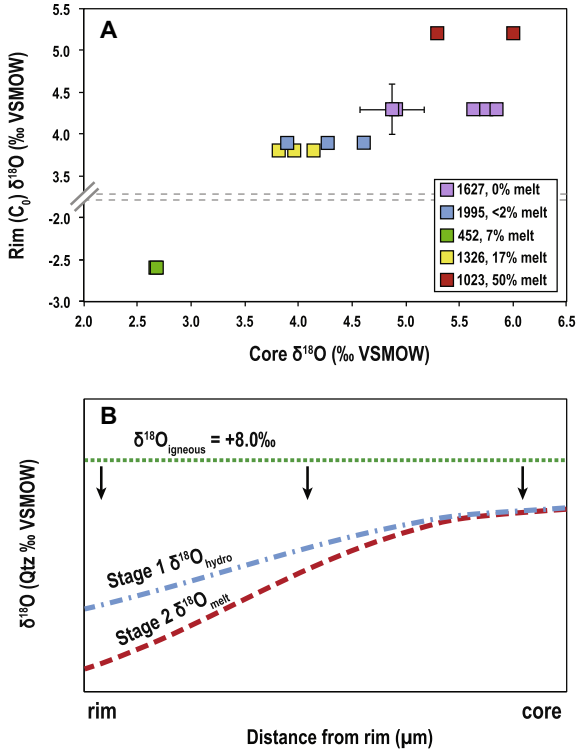

Fig. 7. (A) $\delta^{18}O$ values for the cores (measured) versus re-equilibrated $\delta^{18}O$ (rim) values (calculated) for Exchange Stage 1 in the nonmelted and partially melted samples. Representative error bars (average 2SD = ±0.3‰) have been included for one crystal in sample 1627. (B) Schematic diagram of the two-stage model for producing the oxygen isotope profiles in the partially melted granitoids. The green line represents the initial igneous $\delta^{18}O$ value (C_1). Blue curve represents the oxygen isotope profile after Exchange Stage 1 and the red curve, Exchange Stage 2. (For interpretation of the references to color in this figure legend, the reader is referred to the web version of this article.)

initial/re-equilibration conditions used for each sample is given in Table 2.

6.2.2. Diffusion model results: timescales for hydrothermal exchange (Exchange Stage 1)

The timescales for Exchange Stage 1 for specific samples vary depending on their oxygen isotope profiles and the oxygen isotope composition measured in plagioclase (Fig. 8), as noted above. Self-diffusion models for oxygen isotope zonation measured in quartz transects predict that hydrothermal exchange (Exchange Stage 1) in the nonmelted sample could have occurred over a period of ~1000–63,000 yrs prior to the caldera-forming eruption at temperatures of 700–510 °C, as constrained by transects measured across the largest quartz grain from nonmelted granitoid sample 1627. In the partially melted samples, models suggest that Exchange Stage 1 occurred over a period of ~150 yrs (700 °C, sample 1326) to ~99,000 yrs (510 °C, sample 1995) prior to partial melting. Shorter times calculated for the partially melted samples relative to the nonmelted sample may be the result of shortening of core to rim distances during partial melting. Samples

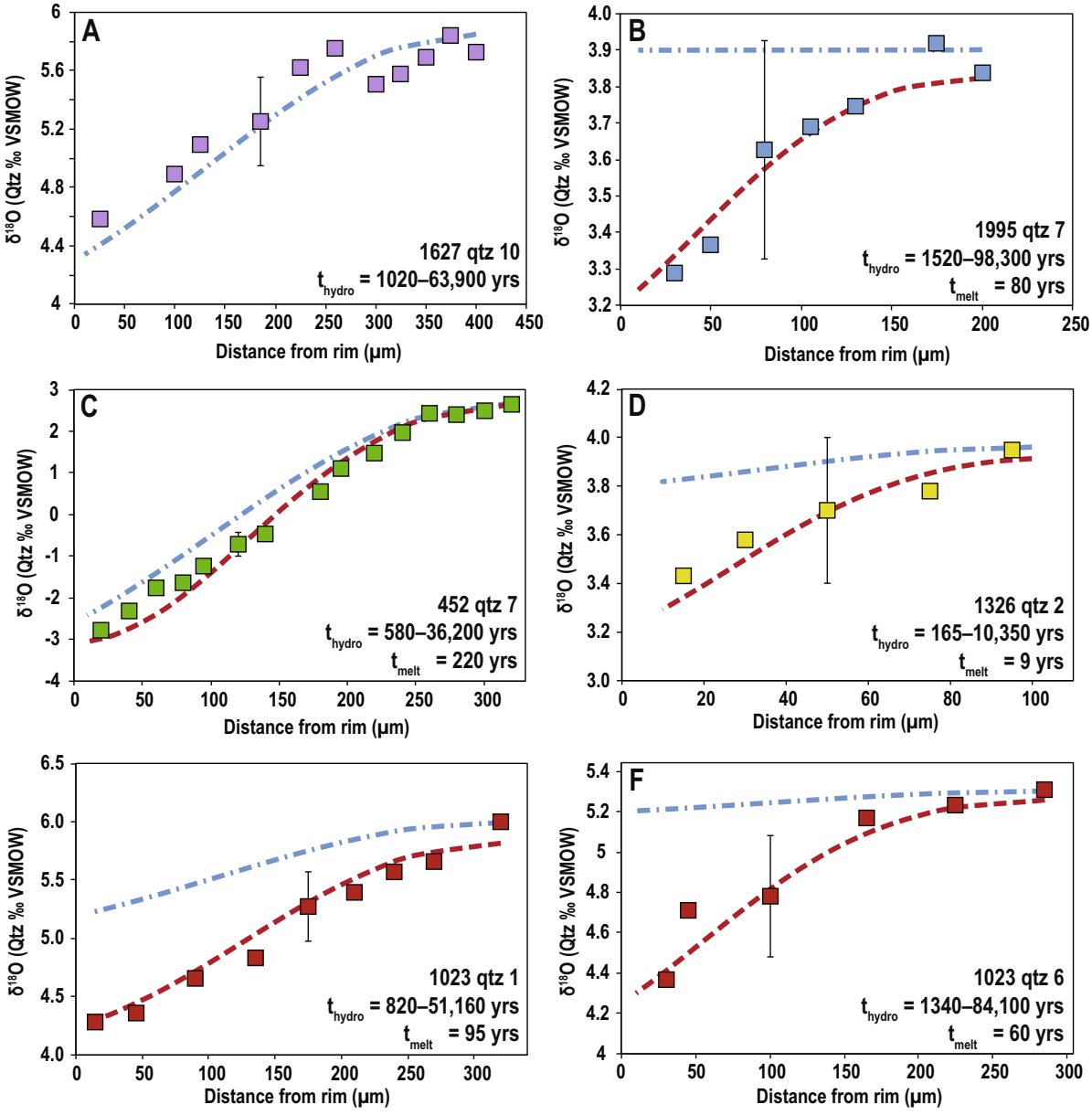

Fig. 8. Modeled diffusion profiles for six SIMS transects in quartz. The blue dotted lines show modeled profiles for hydrothermal exchange (Exchange Stage 1) and the red dotted lines show profiles calculated for high-temperature exchange during partial melting (Exchange Stage 2). Average precision for SIMS values of $\delta^{18}O$ are 0.3‰ (2SD) and are plotted for one spot in each transect. The modeled diffusion profiles are calculated for a spherical model of Crank (1975) and diffusion coefficients for quartz where $P_{H2O} = 100$ MPa (hydrothermal; Dennis, 1984) and $P_{H2O} = 5$ MPa (Farver and Yund, 1991). SIMS data taken from a transect in quartz in sample 1627 (A), a transect in sample 1995 (B), a transect in sample 452 (C), a transect in sample 1326 (D), and two transects in 1023 (E and F), to represent the range of oxygen isotope exchange timescales observed at Mt. Mazama. (For interpretation of the references to color in this figure legend, the reader is referred to the web version of this article.)

Table 2
Oxygen isotope self diffusion modeling parameters.

Sample	T_{hydro} (°C)	T_{melt} (°C)	D_{hydro} (cm^2/s, 510 °C)	D_{hydro} (cm^2/s, 700 °C)	D_{melt} (cm^2/s)	C_1	$C_{0,hydro}$	$C_{0,melt}$
1627	510–700	–	1.25E−16	7.83E−15	–	8.0	4.3	–
1995	510–700	900	1.25E−16	7.83E−15	1.08E−14	8.0	3.9	3.2
452	510–700	842	1.25E−16	7.83E−15	5.17E−15	8.0	−2.6	−3.1
1326	510–700	954	1.25E−16	7.83E−15	2.01E−14	8.0	3.8	3.2
1023	510–700	965	1.25E−16	7.83E−15	2.27E−14	8.0	5.2	4.3

for which we calculated times longer than 63,000 yrs include those in Fig. 6 that require anomalously long times for Exchange Stage 1 despite their relatively small diameters. This means that it is likely more appropriate to assume that the cores of these samples did not reach their current $\delta^{18}O$ values during Exchange Stage 1, but were affected by additional oxygen isotope exchange during Exchange Stage 2. We note that this is necessary to explain the low $\delta^{18}O$ values we measure for sample 1995, which is interpreted as the plutonic equivalent to rhyodacites erupted ~27 ka (Bacon and Lowenstern, 2005) and would require that hydrothermal exchange occurred over timescales of less than ~20,000 yrs.

6.2.3. ^{238}U enrichment and the hydrothermal history of the climactic magma chamber

The combination of U-Th and oxygen isotope data also allows us to evaluate the source and age of U enrichment in the granitoids, particularly as it relates to the hydrothermal system that was associated with the growing upper crustal magma chamber at Mt. Mazama. Here, we further explore the proposal of Ankney et al. (2013) that U enrichment in the granitoids reflects exchange with hydrothermal fluids, a scenario that has been recognized at other caldera settings, including Long Valley, Valles, Timber Mountain, and Yellowstone (Bindeman et al., 2006; Sturchio et al., 1986, 1987; Wollenberg et al., 1995), as well as more generally in arc volcanic systems (e.g., Villemant et al., 1996; Zellmer et al., 2014). Uranium enrichment via meteoric fluid flow has also been documented for the Idaho Batholith, where the greatest enrichment in fluid-mobile elements, including U, occurred in portions of the batholith that had the greatest lowering of δD and $\delta^{18}O$ values (Criss and Taylor, 1983; Gosnold, 1987).

At Mount Mazama, ^{238}U-excess is more common than ^{230}Th excess (Ankney et al., 2013). This is in contrast to other Cascade volcanoes for which U-excess is observed in less than 15% of samples analyzed for U-Th isotopes (Bennett et al., 1982; Newman et al., 1986; Volpe and Hammond, 1991; Volpe, 1992; Jicha et al., 2009; Mitchell and Asmerom, 2011; Wende et al., 2015). Typically, U excess in arc settings is attributed to U addition from dehydration of the subducting slab and fluid fluxing of the mantle wedge, reflecting the fluid-mobile nature of U (e.g., Turner et al., 2003). In the Cascades, U enrichment due to interaction with subduction fluids is thought to be less pronounced than in most other arcs, considering the relatively hot and dry nature of the subduction zone (Wilson, 1988; Blackwell et al., 1990; Harry and Green, 1999; Van Keken et al., 2002; Hildreth, 2007). In a previous study, Ankney et al. (2013) proposed that U excess documented in lavas and pyroclastic rocks erupted from the climactic magma chamber of Mt. Mazama was generated by assimilation of an upper crustal component that was enriched in U through interaction with hydrothermal fluids. The new U-Th isotope data measured in the granitoids in this study support that interpretation, because the $\delta^{18}O$ values of the granitoids have all been lowered from their primary magmatic oxygen isotope compositions, and the granitoids generally fall along a U excess array that is similar to that defined by the preclimactic and climactic dacites and rhyodacites (Fig. 3). Importantly, five of the analyzed granitoids have ^{238}U excesses equal to or greater than any of the dacites or rhyodacites previously analyzed for U-Th isotopes. Sample 452, in particular, has the highest U excess yet measured in a dacite or rhyodacite rock at Mt. Mazama and also has the lowest $\delta^{18}O$ value measured in this study.

The U excess array measured in the granitoids and in volcanic rocks from Mt. Mazama suggests that U enrichment occurred ~40–75 kyrs prior to the climactic eruption (i.e., ~48–83 ka), based on calculations by Ankney et al. (2013) for volcanic rocks and the relations in Fig. 3. The beginning of hydrothermal circulation may be associated with voluminous dacite eruptions at Mt. Mazama that occurred around 70 ka (Bacon and Lanphere, 2006), and we suggest that this records when a persistent upper crustal magma chamber had been developed, which would supply a large shallow heat source to support a hydrothermal envelope. The U-excess timescale for Exchange Stage 1 overlaps with that calculated using the oxygen diffusion models discussed in Section 6.2.1 above, and allows us to put further constraints on the range of t_{hydro} and temperature conditions for Exchange Stage 1. A minimum age of ~48 ka for the onset of hydrothermal circulation would require temperatures of <~525 °C for the nonmelted sample. Assuming a maximum age of ~70 ka per the discussion in Section 6.2.1, we can then propose a fairly narrow range of temperatures for Exchange Stage 1 from ~510 to 525 °C. This is consistent with the $\Delta^{18}O_{qtz\text{-}plag}$ fractionation (using quartz rims) of ~1.6‰ measured for nonmelted sample 1627.

Although the correlation between U excesses and low $\delta^{18}O$ values broadly supports the model of Ankney et al. (2013), two issues must be addressed. The first is that timescales of >40 kyrs are too long to explain the U excess and low-$\delta^{18}O$ values measured in partially melted sample 1995, which zircon geochronology indicates probably had crystallized by ~30 ka (Bacon and Lowenstern, 2005). The presence of zircons with "normal" magmatic $\delta^{18}O$ values in this sample implies that the other minerals in this rock must have experienced subsolidus oxygen isotope exchange during Exchange Stage 1, which can occur at timescales of <20 kyrs according to modeling in Section 6.2.2. The U-Th isotope composition of sample 1995, however, is within error of compositions measured for possible volcanic equivalents by Ankney et al. (2013), which have U excesses that they attribute to assimilation of U-enriched upper crust. We therefore suggest that sample 1995 may have, in part, acquired its U excess from assimilation of earlier granitoids. This is permissible given the higher Fe-Ti oxide temperatures measured for the likely volcanic equivalent of sample 1995 (850 °C, Druitt and Bacon, 1989) relative to those indicated for the original crystallization conditions of earlier granitoids (690–830 °C, Bacon, 1992). The second issue is two granitoid samples that plot in Th excess (Fig. 3) that have low $\delta^{18}O$ values. If our model for U-enrichment due to hydrothermal circulation is correct, presumably through U leaching from other rocks, it is in fact not surprising that some granitoids are in Th excess (as are, presumably, some country rocks). Extensive interaction with hydrothermal

fluids that leached U may account for the high abundance of possible alteration features observed in CL images of quartz in sample 1627 (Fig. B10 in Appendix B), which has the largest Th excess (Fig. 3) relative to others analyzed in this study.

6.3. Timescales for partial melting (Exchange Stage 2)

6.3.1. Parameters for modeling oxygen isotope exchange during partial melting (Exchange Stage 2)

In the partially melted samples, models of high temperature exchange during partial melting (Exchange Stage 2) were calculated by applying Eq. (1) to the initial profiles from Exchange Stage 1 discussed in Section 6.2.2 (Fig. 7b, Table 2). Determining appropriate diffusion coefficients for modeling Exchange Stage 2 was more challenging relative to Exchange Stage 1, because the water contents that existed during melting of the granitoids are difficult to constrain. Oxygen self-diffusion coefficients for quartz vary dramatically depending on the presence of water (e.g., Farver and Yund, 1991). Diffusion coefficients for oxygen diffusion determined in anhydrous studies, where experiments involve exchange with dry-$^{18}O_2$ gas (e.g., Dennis, 1984), are several orders of magnitude smaller than those measured for oxygen diffusion determined for hydrothermal (wet) conditions, where experiments are typically performed at a pressure of water (P_{H2O}) of 100 MPa (e.g., Dennis, 1984; Giletti and Yund, 1984; Sharp et al., 1991). Because the granitoids at Mt. Mazama underwent exchange with hydrothermal fluids during Exchange Stage 1, and contain abundant aqueous fluid inclusions in quartz and feldspar, water activity may have been high during melting, although the melts evidently were not water-saturated, especially in samples with higher melt fractions (Bacon, 1992; Bacon et al., 1994). Moreover, Fe-Ti oxide geothermometry and water contents of glass suggest that partial melting occurred without introduction of a vapor phase (Bacon, 1992). We therefore calculated high-temperature diffusion profiles and timescales (t_{melt}) for Exchange Stage 2 in the partially melted samples using diffusion coefficients for quartz for both anhydrous (Dennis, 1986) and hydrothermal conditions (Dennis, 1984). At temperatures of ~850–1000 °C, these values of D require $t_{melt} = \sim$1500–90,000 years (anhydrous) and $t_{melt} \geq \sim$1 year (hydrothermal). We suggest that the actual diffusion coefficients for the granitoids during partial melting likely fall somewhere in between values determined for anhydrous and hydrothermal conditions as there would have been some water dissolved in melts, and we therefore favor values from Farver and Yund (1991), who measured rates of oxygen self-diffusion in quartz over a range of P_{H2O} from 5 to 350 MPa. It is important to note that the addition of only a small amount of water ($P_{H2O} = 5$ MPa) increases the diffusion coefficient for quartz relative to an anhydrous value by at least two orders of magnitude. Additional parameters and results for models using diffusion coefficients for Exchange Stage 2 where $P_{H2O} = 5$ MPa, which is appropriate given the low water content of the partial melts of the Crater Lake granitoids (<1 wt.%), are discussed in detail below.

Diffusion coefficients for Exchange Stage 2 were adjusted for different temperatures on a sample-specific basis using Eq. (2). Farver and Yund (1991) do not give D_0 and E for the variable P_{H2O} experiments, so in order to scale diffusion coefficients with temperature for partial melting, we back-calculated the pre-exponential factor using the experimental temperature of 700 °C and an activation energy of 138 kJ/mol, which is equal to an experimental value for quartz determined by Dennis (1984). We note that this value for E is relatively low in comparison to most others found in the experimental literature (e.g., Dennis, 1984; Giletti and Yund, 1984; Farver and Yund, 1991; Sharp et al., 1991; Farver, 2010), so it provides a conservative estimate of the increase in diffusion coefficients with increasing temperature. Temperatures equal to Fe-Ti oxide temperatures determined by Bacon (1992) for re-equilibrated oxides in contact with glass were used to calculate diffusion coefficients for quartz in the partially melted granitoids, with the exception of sample 1995 for which there are no oxide temperatures available. For this sample, we assumed a temperature of 900 °C, which is a moderate value for a partially melted granitoid and is reasonable given its $\Delta^{18}O_{qtz\text{-}plag}$ fractionation (for quartz rims) of 0.9‰.

The amount of time (t_{melt}) required for Exchange Stage 2 can also vary based on the extent of oxygen isotope exchange that is presumed to have occurred during Exchange Stage 1. As noted above in Section 6.2.1, the initial (C_1) profiles for the partially melted samples were calculated assuming that the core of each crystal reached its current value during Exchange Stage 1. Values for C_0 during partial melting were estimated based on appropriate high-temperature equilibrium values with glass (bulk values from Bacon et al., 1989) and/or plagioclase. This gives maximum possible ages for Exchange Stage 1, and therefore results in minimum ages for Exchange Stage 2. Maximum ages for Exchange Stage 2 can be calculated by assuming the quartz crystals were unaffected by oxygen isotope exchange during Exchange Stage 1, i.e., they had no oxygen isotope zonation present prior to partial melting and were in equilibrium with zircon ($\delta^{18}O_{qtz} = +8.0$‰). We calculate maximum ages of $t_{melt} = \sim$30–840 years for the partially melted samples, which, although longer than those discussed below, do not markedly change our interpretations of the high temperature (Exchange Stage 2) history of the granitoids with respect to the growing climactic magma chamber.

6.3.2. Diffusion model results: timescales for partial melting (Exchange Stage 2)

The onset of melting (Exchange Stage 2) in the partially melted granitoids is predicted by our models to have occurred at a minimum of ~10–200 years prior to the climactic eruption of Mt. Mazama (Fig. 8). We propose that the age for Exchange Stage 2 represents the timing of a temperature increase of the climactic magma chamber, likely due to the addition of heat and volume from the injection of the final batches of mafic recharge magma into the chamber prior to the caldera-forming eruption. Timescales of 10s–100s of years prior to the climactic eruption are

consistent with the final preclimactic rhyodacite eruptions of Llao Rock at ~7.9 ka and Cleetwood at ~7.7–7.8 ka (Bacon and Lanphere, 2006). Iron-titanium oxide temperatures and stratigraphic relations imply that the higher-temperature, partially melted granitoids were derived from the deeper walls of the climactic magma chamber, suggesting that they were likely situated in close proximity to recharge magma and associated mafic cumulates (Druitt and Bacon, 1989; Bacon, 1992). Compositions and textures of enclaves in the Llao Rock and Cleetwood lavas, and of scoria in climactic ejecta are supportive of injection of multiple batches of recharge magma into the chamber during the final buildup to the climactic eruption (Bacon and Druitt, 1988; Druitt and Bacon, 1989). The isotopic and trace-element composition of HSr enclaves found in the Llao Rock rhyodacite differs from those found in the Cleetwood rhyodacite, suggesting that they interacted with different batches of recharge magma (Bacon and Druitt, 1988; Bacon et al., 1994). Moreover, some plagioclase phenocrysts found in HSr scoria from the climactic eruption have compositions and disequilibrium textures (spongy, corroded) that are consistent with injection of hotter, HSr recharge magma into the cumulate pile below the convecting rhyodacite magma within the climactic magma chamber (Druitt and Bacon, 1989). Based on these lines of evidence, melting of the granodiorites, and high-temperature oxygen isotope exchange (Exchange Stage 2) within a conductive thermal boundary surrounding the magma chamber, seems likely to record the timing of these or similar recharge events.

The timescales calculated for oxygen isotope exchange for partial melting can be tested against Fe-Ti oxide re-equilibration timescales for the granitoid blocks based on the spherical model for diffusion of Crank (1975) and diffusion coefficients for Ti calculated from equation 21 of Aragon et al. (1984) (Fig. 9). Bacon (1992) indicates that the timing of Fe-Ti oxide re-equilibration in the partially melted samples represents a minimum time for the duration of melting in the granitoids. He suggests that melting initiated hundreds of years prior to the caldera-forming eruption, based on calculations of diffusion of Ti in titanomagnetite (the rate-limiting step in oxide re-equilibration, Aragon et al., 1984) for the lowest temperature partially melted granitoid block (760–790 °C) and the largest magnetite crystals (200 μm). The times required for isothermal homogenization of the largest magnetites (200 μm) for our samples range from 200 to 10 years and are consistent with times calculated for oxygen isotope exchange in the quartz, assuming a $P_{H2O} = 5$ MPa (Fig. 9). In the two samples that contain the highest vol. % melt, the Fe-Ti oxide times are at the lower end or below the range of the oxygen isotope exchange. This may suggest that the Fe-Ti oxides re-equilibrated early during heating ± partial melting of the granitoids, and then were stored at high temperatures for some period of time prior to eruption.

La Tourrette et al. (1991) determined minor and trace element concentrations in Fe-Ti oxides, zircon, and glass in three partially melted granodiorite samples from Crater Lake. They found no difference in Zr concentration in glass

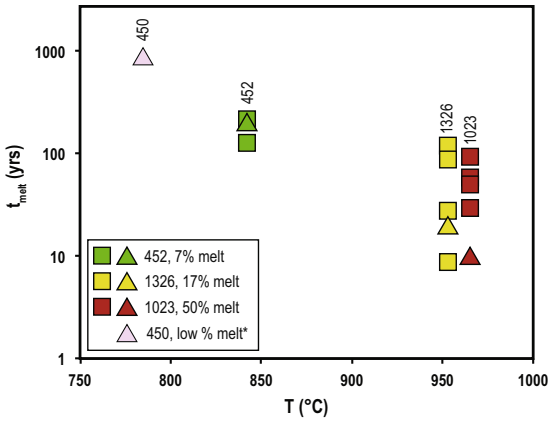

Fig. 9. Comparison of oxygen diffusion timescales for Exchange Stage 2 for the SIMS transects in quartz (this study, squares) and Ti diffusion timescales in magnetite from Fe-Ti oxide thermometry (triangles) of Bacon (1992). Parameters used to calculate the timescales are described in the text. Fe-Ti oxide temperatures are from Bacon (1992). * denotes the inclusion of Fe-Ti oxide data for sample 450 from Bacon (1992), which represents the lowest temperature partially melted sample found at Mt. Mazama.

<100 μm and >500 μm from zircon in sample 1326, but reported Zr concentrations in two higher-melt-fraction samples, 1038 and one not analyzed in our study, that were significantly higher near zircon than >500 μm away. Assuming that the measured Zr differences reflect diffusion away from zircon dissolving in low-H_2O rhyolitic melt, the Zr data were interpreted to suggest that the samples could have been partially molten for 800–8000 yrs. The times predicted by diffusion models for oxygen isotopes in quartz are probably a more accurate representation of the onset and duration of melting prior to eruption than those based on Fe-Ti oxide homogeneity or Zr gradients in glass, especially because the preservation of diffusion profiles in quartz provides robust constraints on the diffusion models.

7. AN "OUTSIDE IN VIEW OF THE MAGMA CHAMBER AT MT. MAZAMA

Oxygen and U-Th isotopes measured in the granitoid wall rocks allow us to characterize the environment of the magma chamber at Mt. Mazama, from the early hydrothermal envelope to recharge leading up to the caldera-forming eruption (Fig. 10). Exchange Stage 1, which includes hydrothermal circulation and U enrichment of the granitoids, likely initiated between 48 and 70 ka, based on the eruptive history of evolved Mazama magmas (Bacon et al., 1989; Bacon and Lanphere, 2006), U-Th data for volcanic rocks (Ankney et al., 2013), and new oxygen and U-Th isotope data for the granitoid wall rocks. At ~27 ka, the first preclimactic rhyodacite eruptions occurred (Bacon and Lanphere, 2006), which are thought to have marked the establishment of the large, silicic upper crustal magma chamber that eventually fed the caldera-forming eruption at Mt. Mazama (Bacon and Druitt, 1988). A portion of the rhyodacite magma associated with these eruptions is interpreted to have crystallized at the margins

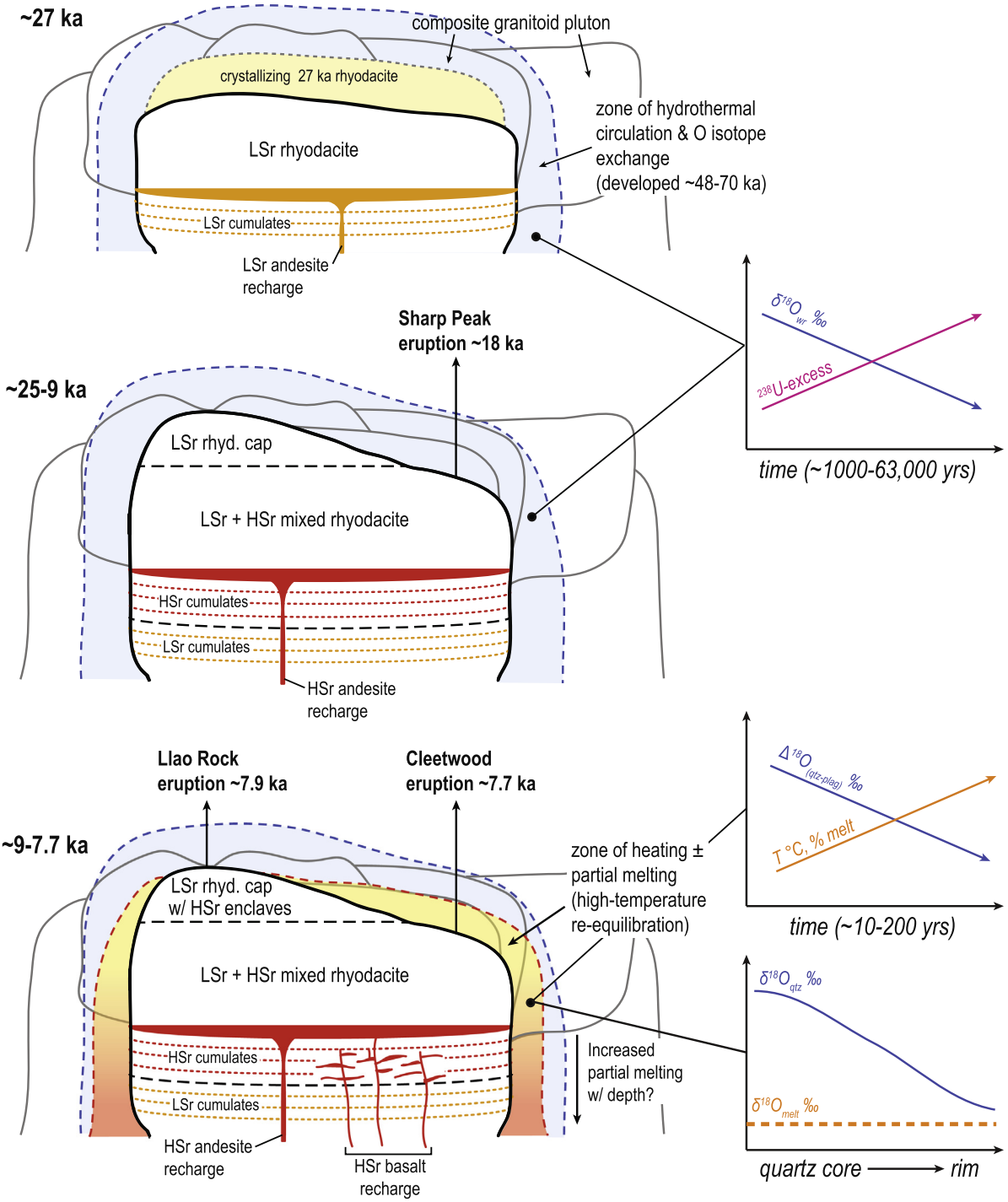

Fig. 10. Summary of the thermal and fluid history of the granitoid blocks ejected during the climactic eruption, and changes in their U-Th and oxygen isotope compositions, throughout the buildup to the caldera-forming eruption at 7.7 ka. A detailed summary of the processes depicted here can be found in the text. The timescales indicated are based on modeling of U-enrichment via hydrothermal fluids and oxygen isotope exchange and Fe-Ti oxide re-equilibration due to heating and partial melting. We note that temperature increases and associated heating, partial melting, and assimilation of the wall rocks of the climactic chamber likely occurred throughout the time period depicted here, but partial melting of the blocks analyzed in this study apparently did not occur until 10^1–10^2 years prior to the caldera-forming eruption. Figure is modified from Druitt and Bacon (1989).

of the growing climactic magma chamber (Bacon and Lowenstern, 2005), as represented in this study by granitoid sample 1995, which has a U-Th zircon age of ~30 ka and contains zircon crystals that have younger nominal model ages (Bacon and Lowenstern, 2005). Notably, we measured low-$\delta^{18}O$ values in quartz and plagioclase for this sample, indicating that the hydrothermal envelope was capable of producing significant changes in oxygen isotope

compositions over periods of 10^3 to 10^4 years, and as recently as the Last Glacial Maximum (Fig. 10).

Eruption of the Llao Rock rhyodacite at ~7.9 ka brought an end to a >10 kyr period of repose in silicic eruptive activity at Mt. Mazama (Bacon and Lanphere, 2006). It was followed shortly by eruption of the Cleetwood rhyodacite at ~7.7–7.8 ka and the climactic eruption at 7.7 ka. Oxygen isotope exchange timescales, as well as high Fe-Ti oxide temperatures, indicate that Exchange Stage 2, heating and partial melting of the granitoid rocks, began as little as $\sim10^1$ to 10^2 years prior to the caldera-forming eruption. We suggest that these timescales correlate with a temperature increase at the magma-wall rock interface in response to mafic recharge (Fig. 10). The recharge magmas, which pooled at the base of the large volume of accumulated rhyodacite magma, or also were injected into the mafic cumulate pile deeper in the chamber (Druitt and Bacon, 1989), provided the heat required to partially melt granitoid wall rocks. This may have contributed to destabilization of the upper part of the magma chamber, possibly leading to the caldera-forming eruption.

8. CONCLUSIONS

This study documents shifts in the oxygen and U-Th isotope compositions of granitoid wall rocks in response to thermal events in the climactic magma chamber of Mt. Mazama, including the onset and duration of hydrothermal circulation, as well as heating due to recharge leading up to the caldera-forming eruption. Timescales for U enrichment measured in the granitoids and models of oxygen isotope exchange in nonmelted to minimally melted samples suggest that hydrothermal exchange associated with the climactic magma chamber initiated ~48–70 ka and was capable of producing core-rim zonation in quartz in 10^3 to 10^4 years (Exchange Stage 1). In partially melted granitoids, models indicate that zoning in quartz developed rapidly over timescales of 10^1 to 10^2 years (Exchange Stage 2). Although our models envision these isotopic shifts as the result of a two-stage process, we stress that it is more likely that they developed over a minimum of two stages, including hydrothermal and partial melting processes. Importantly, our results add to a growing body of evidence that destabilization of large silicic magma chambers via recharge may occur within decades preceding caldera-forming eruptions (e.g., Michaut and Jaupart, 2006; Wark et al., 2007; Saunders et al., 2010; Druitt et al., 2012). The unique "outside in" view of this process provided is distinct from the record that may be preserved (or perhaps be absent) in the phenocrysts in juvenile erupted magma.

ACKNOWLEDGMENTS

We thank Kouki Kitajima, Brian Hess, Jim Kern, Mike Spicuzza, Noriko Kita and others in the WiscSIMS Laboratory at the University of Wisconsin-Madison Department of Geoscience for their assistance in preparing and analyzing samples for oxygen isotope ratios. Mike Spicuzza assisted in oxygen isotope analysis by laser fluorination. We also thank John Fournelle and Phil Gopon for help in imaging and analyzing samples via SEM and EPMA. Additionally, we acknowledge Allison Wende for her assistance with U-Th isotope analyses. This manuscript benefited from thoughtful reviews by Kathryn Watts, Ilya Bindeman, Georg Zellmer, and Paul Tomascak, as well as editing by James Day. This work was supported by National Science Foundation Grant No. EAR-1144937, as well as the National Science Foundation Graduate Research Fellowship program under Grant No. DGE-0718123. WiscSIMS is partly supported by NSF-EAR-1053466, -1355590.

APPENDIX A. SUPPLEMENTARY MATERIAL

Supplementary data associated with this article can be found, in the online version, at http://dx.doi.org/10.1016/j.gca.2017.04.043.

REFERENCES

Allan A. S. R., Morgan D. J., Wilson C. J. N. and Millet M.-A. (2013) From mush to eruption in centuries: assembly of the super-sized Oruanui magma body. *Contrib. Miner. Petrol.* **166**, 143–164.

Ankney M. E., Johnson C. M., Bacon C. R., Beard B. L. and Jicha B. R. (2013) Distinguishing lower and upper crustal processes in magmas erupted during the buildup to the 7.7 ka climactic eruption of Mount Mazama, Crater Lake, Oregon, using 238U–230Th disequilibria. *Contrib. Miner. Petrol.* **166**, 563–585.

Aragon R., McCallister R. H. and Harrison H. R. (1984) Cation diffusion in titanomagnetites. *Contrib. Miner. Petrol.* **85**, 174–185.

Arzi A. A. (1978) Critical phenomena in the rheology of partially melted rocks. *Tectonophysics* **44**, 173–184.

Bachmann O., Oberli F., Dungan M. A., Meier M., Mundil R. and Fischer H. (2007) $^{40}Ar/^{39}Ar$ and U-Pb dating of the Fish Canyon magmatic system, San Juan Volcanic field, Colorado: evidence for an extended crystallization history. *Chem. Geol.* **236**, 134–166.

Bacon C. R. (1992) Partially melted granodiorite and related rocks ejected from Crater Lake caldera, Oregon. *Trans. R. Soc. Edinburgh, Earth Sci.* **83**, 27–47.

Bacon C. R. (2008) Geologic map of Mount Mazama and Crater Lake Caldera, Oregon: U.S. Geological Survey Scientific Investigations Map 2832, 4 sheets, scale 1:24,000, p. 45 p. pamphlet.

Bacon C. R. and Druitt T. H. (1988) Compositional evolution of the zoned calcalkaline magma chamber of Mount Mazama, Crater Lake, Oregon. *Contrib. Miner. Petrol.* **98**, 224–256.

Bacon C. R. and Lanphere M. A. (2006) Eruptive history and geochronology of Mount Mazama and the Crater Lake region, Oregon. *Geol. Soc. Am. Bull.* **118**, 1331–1359.

Bacon C. R. and Lowenstern J. B. (2005) Late Pleistocene granodiorite source for recycled zircon and phenocrysts in rhyodacite lava at Crater Lake, Oregon. *Earth Planet. Sci. Lett.* **233**, 277–293.

Bacon C. R., Adami L. H. and Lanphere M. A. (1989) Direct evidence for the origin of low-^{18}O silicic magmas: quenched samples of a magma chamber's partially-fused granitoid walls, Crater Lake, Oregon. *Earth Planet. Sci. Lett.* **96**, 199–208.

Bacon C. R., Gunn S. H., Lanphere M. A. and Wooden J. L. (1994) Multiple isotopic components in Quaternary volcanic rocks of the Cascade arc near Crater Lake, Oregon. *J. Petrol.* **35**, 1521–1556.

Bacon C. R., Persing H. M., Wooden J. L. and Ireland T. R. (2000) Late pleistocene granodiorite beneath Crater Lake caldera, Oregon, dated by ion microprobe. *Geology* **28**, 467–470.

Bennett J. T., Krishnaswami S., Turekian K. K., Melson W. G. and Hopson C. A. (1982) The uranium and thorium decay series nuclides in Mt. St. Helens effusives. *Earth Planet. Sci. Lett.* **60**, 61–69.

Bindeman I. and Simakin A. G. (2014) Rhyolites-Hard to produce, but easy to recycle and sequester: integrating microgeochemical observations and numerical models. *Geosphere* **10**, 930–957.

Bindeman I. N. and Valley J. W. (2002) Oxygen isotope study of the Long Valley magma system, California: isotope thermometry and convection in large silicic magma bodies. *Contrib. Miner. Petrol.* **144**, 185–205.

Bindeman I. N., Schmitt A. K. and Valley J. W. (2006) U-Pb zircon geochronology of silicic tuffs from the Timber Mountain/Oasis Valley caldera complex, Nevada: rapid generation of large volume magmas by shallow-level remelting. *Contrib. Miner. Petrol.* **152**, 649–665.

Blackwell D. D., Steele J. L. and Kelley S. (1990) Heat flow in the State of Washington and thermal conditions in the cascade range. *J. Geophys. Res.* **95**, 19495–19516.

Brown S. J. A. and Fletcher I. R. (1999) SHRIMP U-Pb dating of the preeruption growth history of zircons from the 340 ka Whakamaru Ignimbrite, New Zealand: evidence for >250 k.y. magma residence times. *Geology* **27**, 1035–1038.

Bruggman P. E., Bacon C. R., Aruscavage P. J., Lerner R. W., Schwarz, L. J. and Stewart K. C. (1987) Chemical analyses of rocks and glass separates from Crater Lake National Park and vicinity, Oregon. U.S. Geological Survey Open-File Report 87-57, 38.

Chiba H., Chacko T., Clayton R. N. and Goldsmith J. R. (1989) Oxygen isotope fractionations involving diopside, forsterite, magnetite, and calcite: application to geothermometry. *Geochim. Cosmochim. Acta* **53**, 2985–2995.

Crank J. (1975) *The Mathematics of Diffusion*. Claredon Press, Oxford.

Criss R. E. and Taylor, Jr., H. P. (1983) An $^{18}O/^{16}O$ and D/H study of Tertiary hydrothermal systems in the southern half of the Idaho batholith. *Geol. Soc. Am. Bull.* **94**, 640–663.

de Silva S. L., Salas G. and Schubring S. (2008) Triggering explosive eruptions: the case for silicic magma recharge at Huaynaputina, southern Peru. *Geology* **36**, 387–390.

Dennis P. F. (1984) Oxygen self-diffusion in quartz under hydrothermal conditions. *J. Geophys. Res.* **89**, 4047–4057.

Dennis P. F. (1986) Oxygen self diffusion in quartz. NERC.

Druitt T. H. and Bacon C. R. (1989) Petrology of the zoned calcalkaline magma chamber of Mount Mazama, Crater Lake, Oregon. *Contrib. Miner. Petrol.* **101**, 245–259.

Druitt T. H., Costa F., Deloule E., Dungan M. A. and Scaillet B. (2012) Decadal to monthly timescales of magma transfer and reservoir growth at a caldera volcano. *Nature* **482**, 77–82.

Eiler J. M., Baumgartner L. P. and Valley J. W. (1992) Intercrystalline stable isotope diffusion: a fast grain boundary model. *Contrib. Miner. Petrol.* **112**, 543–557.

Elphick S. C., Graham C. M. and Dennis P. F. (1988) An ion probe study of anhydrous oxygen diffusion in anorthite: a comparison with hydrothermal data and some geological implications. *Contrib. Miner. Petrol.* **100**, 490–495.

Farver J. R. (2010) Oxygen and hydrogen diffusion in minerals. *Rev. Mineral. Geochem.* **72**, 447–507.

Farver J. R. and Yund R. A. (1991) Oxygen diffusion in quartz: dependence on temperature and water fugacity. *Chem. Geol.* **90**, 55–70.

Folkes C. B., de Silva S. L., Schmitt A. K. and Cas R. A. F. (2011) A reconnaissance of U-Pb ages in the Cerro Galàn system, NW Argentina: prolonged magma residence, crystal recycling, and crustal assimilation. *J. Volcanol. Geoth. Res.* **206**, 136–147.

Giletti B. J. and Yund R. A. (1984) Oxygen diffusion quartz. *J. Geophys. Res.* **89**, 4039–4046.

Giletti B. J., Semet M. P. and Yund R. A. (1978) Studies in diffusion-III. Oxygen in feldspars: an ion microprobe determination. *Geochim. Cosmochim. Acta* **42**, 45–57.

Gosnold W. D. (1987) Redistribution of U and Th in shallow plutonic environments. *Geophys. Res. Lett.* **14**, 291–294.

Harry D. L. and Green N. L. (1999) Slab dehydration and basalt petrogenesis in subduction systems involving very young oceanic lithosphere. *Chem. Geol.* **160**, 309–333.

Heck P., Huberty J., Kita N. T., Ushikubo T., Kozdon R. and Valley J. W. (2011) SIMS analyses of silicon and oxygen isotope ratios for quartz from Archean and Paleo-proterozoic banded iron formations. *Geochim. Cosmochim. Acta* **75**, 5879–5891.

Hildreth W. (1996) Kulshan caldera: a Quaternary subglacial caldera in the North Cascades, Washington. *Geol. Soc. Am. Bull.* **108**, 786–793.

Hildreth W. (2007) Quaternary magmatism in the Cascades-geologic perspectives. *U.S. Geol. Surv. Prof. Pap.* **1744**, 125.

Jicha B. R., Johnson C. M., Hildreth W., Beard B. L., Hart G. L., Shirey S. B. and Singer B. S. (2009) Discriminating assimilants and decoupling deep- vs. shallow-level crystal records at Mount Adams using ^{238}U–^{230}Th disequilibria and Os isotopes. *Earth Planet. Sci. Lett.* **277**, 38–49.

Kelly J., Fu B., Kita N. T. and Valley J. W. (2007) Optically continuous silcrete quartz cements of the St. Peter Sandstone: high precision oxygen isotope analysis by ion microprobe. *Geochim. Cosmochim. Acta* **71**, 3812–3832.

Kita N. T., Ushikubo T., Fu B. and Valley J. W. (2009) High precision SIMS oxygen isotope analysis and the effect of sample topography. *Chem. Geol.* **264**, 43–57.

Kita N. T., Huberty J. M., Kozdon R., Beard B. L. and Valley J. W. (2011) High-precision SIMS oxygen, sulfur and iron stable isotope analyses of geological materials: accuracy, surface topography and crystal orientation. *Surf. Interf. Anal.* **43**, 427–431.

La Tourrette T. Z., Burnett D. S. and Bacon C. R. (1991) Uranium and minor-element partitioning in Fe-Ti oxides and zircon from partially melted granodiorite, Crater Lake, Oregon. *Geochim. Cosmochim. Acta* **55**, 457–469.

Marsh B. D. (1981) On the crystallinity, probability of occurrence, and rheology of lava and magma. *Contrib. Miner. Petrol.* **78**, 85–98.

Matthews A., Goldsmith J. R. and Clayton R. N. (1983) Oxygen isotope fractionation involving pyroxenes: the calibration of mineral-pair geothermometers. *Geochim. Cosmochim. Acta* **47**, 645–654.

Michaut C. and Jaupart C. (2006) Ultra-rapid formation of large volumes of evolved magma. *Earth Planet. Sci. Lett.* **250**, 38–52.

Mitchell E. C. and Asmerom Y. (2011) U-series isotope systematics of mafic magmas from central Oregon: implications for fluid involvement and melting processes in the Cascade arc. *Earth Planet. Sci. Lett.* **312**, 378–389.

Newman S., Macdougall J. D. and Finkel R. C. (1986) Petrogenesis and ^{230}Th-^{238}U disequilibrium at Mt. Shasta, California, and in the Cascades. *Contrib. Miner. Petrol.* **93**, 195–206.

Peres P., Kita N. T., Valley J. W., Fernandes F. and Schumacher M. (2013) New sample holder geometry for high precision isotope analyses. *Surf. Interf. Anal. (SIMS Proc.)* **45**, 553–556.

Saunders K. E., Morgan D. J., Baker J. A. and Wysoczanski R. J. (2010) The magmatic evolution of the Whakamaru Supereruption, New Zealand, constrained by a microanalytical study of plagioclase and quartz. *J. Petrol.* **51**, 2465–2488.

Sharp Z. D., Giletti B. J. and Yoder, Jr., H. S. (1991) Oxygen diffusion rates in quartz exchanged with CO_2. *Earth Planet. Sci. Lett.* **107**, 338–348.

Simon J. I. and Reid M. R. (2005) The pace of rhyolite differentiation and storage in an 'archetypical' silicic magma system, Long Valley, California. *Earth Planet. Sci. Lett.* **235**, 123–140.

Sims K. W. W., Gill J., Dosseto A., Hoffman D. L., Lundstrom C. C., Williams R. W., Ball L., Tollstrup D., Turner S., Prytulak J., Glessner J. J. G., Standish J. J. and Elliott T. (2008) An inter-laboratory assessment of the thorium isotopic composition of synthetic and rock reference materials. *Geostand. Geoanal. Res.* **32**, 65–91.

Sturchio N. C., Binz C. M. and Lewis, III, C. H. (1987) Thorium-uranium disequilibrium in a geothermal discharge zone at Yellowstone. *Geochim. Cosmochim. Acta* **51**, 2025–2034.

Sturchio N. C., Muehlenbachs K. and Seitz M. G. (1986) Element redistribution during hydrothermal alteration of rhyolite in an active geothermal system: yellowstone drill cores Y-7 and Y-8. *Geochim. Cosmochim. Acta* **50**, 1619–1631.

Thompson J. M., White L. D. and Nathenson M. (1987) *Chemical analyses of waters from Crater Lake, Oregon, and nearby springs*. U.S. Geological Survey Open-File Report, p. 16.

Turner S., Bourdon B. and Gill J. (2003) Insights into magma genesis at convergent margins from U-series isotopes, In Uranium-Series Geochemistry (eds. B. Bourdon, G.M. Henderson, C. C. Lundstrom and S. P. Turner). Reviews in Mineralogy and Geochemistry. pp. 255–315.

Valley J. W. (2001) Stable isotope thermometry at high temperatures. *Rev. Mineral. Geochem.* **43**, 365–413.

Valley J. W. (2003) Oxygen isotopes in zircon. *Rev. Mineral. Geochem.* **53**, 343–385.

Valley J. W. and Kita N. T. (2009) *In situ* oxygen isotope geochemistry by ion microprobe. *MAC Short Course: Secondary Ion Mass Spectrom. Earth Sci.* **41**, 19–63.

Van Keken P. E., Kiefer B. and Peacock S. M. (2002) High-resolution models of subduction zones: implications for mineral dehydration reactions and the transport of water into the deep mantle. *Geochem. Geophys. Geosyst.* **3**, 1056.

Vazquez J. A. and Reid M. R. (2004) Probing the accumulation history of the voluminous Toba magma. *Science* **305**, 991–994.

Villemant B., Boudon G. and Komorowski J.-C. (1996) U-series disequilibrium in arc magmas induced by water-magma interaction. *Earth Planet. Sci. Lett.* **140**, 259–267.

Volpe A. M. (1992) ^{238}U–^{230}Th-^{226}Ra disequilibrium in young Mt. Shasta andesites and dacites. *J. Volcanol. Geoth. Res.* **53**, 227–238.

Volpe A. M. and Hammond P. E. (1991) ^{238}U–^{230}Th-^{226}Ra disequilibria in young Mount St. Helens rocks: time constraint for magma formation and crystallization. *Earth Planet. Sci. Lett.* **107**, 475–486.

Wark D., Hildreth W., Spear F. S., Cherniak D. J. and Watson E. B. (2007) Pre-eruption recharge of the Bishop magma system. *Geology* **35**, 235–238.

Wende A. M., Johnson C. M. and Beard B. L. (2015) Tracing changes in mantle and crustal influences in individual cone-building stages at Mt. Shasta using U-Th and Sr isotopes. *Earth Planet. Sci. Lett.* **428**, 11–21.

Wilson D. S. (1988) Tectonic history of the Juan de Fuca Ridge over the last 40 million years. *J. Geophys. Res.* **93**, 11863–11876.

Wollenberg H. A., Flexser S. and Smith A. R. (1995) Mobility and depositional controls of radioelements in hydrothermal systems at the Long Valley and Valles calderas. *J. Volcanol. Geoth. Res.* **67**, 171–186.

Wotzlaw J.-F., Schaltegger U., Frick D. A., Dungan M. A., Gerdes A. and Günther D. (2013) Tracking the evolution of large-volume silicic magma reservoirs from assembly to supereruption. *Geology* **41**, 867–870.

Wotzlaw J.-F., Bindeman I., Watts K. E., Schmitt A. K., Caricchi L. and Schaltegger U. (2014) Linking rapid magma reservoir assembly and eruption trigger mechanisms at evolved Yellowstone-type supervolcanoes. *Geology* **42**, 807–810.

Wotzlaw J.-F., Bindeman I. N., Stern R. A., D'Abzac F.-X. and Schaltegger U. (2015) Rapid heterogeneous assembly of multiple magma reservoirs prior to Yellowstone supereruptions. *Nat. Sci. Rep.* **5**, 14026.

Zellmer G. F., Freymuth H., Cembrano J. M., Clavero J. E., Veloso E. A. E. and Sielfeld G. G. (2014) Altered mineral uptake into fresh arc magmas: insights from U-Th isotopes of samples from Andean volcanoes under differential crustal stress regimes. In *Orogenic Andesites and Crustal Growth* (eds. A. Gómez-Tuena, S. M. Straub and G. F. Zellmer). Geological Society, Special Publications, London, pp. 185–208.

Associate Editor: James M.D. Day